

Supersonic Shear Instabilities in Astrophysical Boundary Layers

Mikhail A. Belyaev¹ & Roman R. Rafikov^{1,2}

ABSTRACT

Disk accretion onto weakly magnetized astrophysical objects often proceeds via a boundary layer that forms near the object's surface, in which the rotation speed of the accreted gas changes rapidly. Here we study the initial stages of formation for such a boundary layer around a white dwarf or a young star by examining the hydrodynamical shear instabilities that may initiate mixing and momentum transport between the two fluids of different densities moving supersonically with respect to each other. We find that an initially laminar boundary layer is unstable to two different kinds of instabilities. One is an instability of a supersonic vortex sheet (implying a discontinuous initial profile of the angular speed of the gas) in the presence of gravity, which we find to have a growth rate of order (but less than) the orbital frequency. The other is a sonic instability of a finite width, supersonic shear layer, which is similar to the Papaloizou-Pringle instability. It has a growth rate proportional to the shear inside the transition layer, which is of order the orbital frequency times the ratio of stellar radius to the boundary layer thickness. For a boundary layer that is thin compared to the radius of the star, the shear rate is much larger than the orbital frequency. Thus, we conclude that sonic instabilities play a dominant role in the initial stages of nonmagnetic boundary layer formation and give rise to very fast mixing between disk gas and stellar fluid in the supersonic regime.

Subject headings: accretion, accretion disks – hydrodynamics — waves – instabilities

1. Introduction

Accretion onto astrophysical objects possessing a material surface (as opposed to accretion onto black holes) always involves a non-trivial interaction of the incoming gas with the object's outer layers. Examples of such objects include white dwarfs in cataclysmic variables (CVs), young stars gaining material from a protoplanetary disk, and accreting neutron stars. In all these systems, one must understand how the incoming gas shares its angular momentum with the accreting object and how it mixes with the previously accreted material.

¹Department of Astrophysical Sciences, Princeton University, Ivy Lane, Princeton, NJ 08540; rrr@astro.princeton.edu

²Sloan Fellow

If the magnetic field of the central object is strong enough, it can disrupt the disk at some distance above the surface. Inside this region, accretion proceeds along field lines (Ghosh & Lamb 1978; Koldoba et al. 2002). The critical value of the magnetic field at the surface of the central object for magnetic disruption is given by

$$B_{*,\text{crit}} = 5 \times 10^4 \left(\frac{\beta}{.5}\right)^{-7/4} \left(\frac{M_*}{.6M_\odot}\right)^{1/4} \left(\frac{\dot{M}}{10^{-8}M_\odot \text{ yr}^{-1}}\right)^{1/2} \left(\frac{R_*}{9 \times 10^3 \text{ km}}\right)^{-5/4} \text{ G.} \quad (1)$$

Here, we have used parameters for the mass and radius that are typical for CVs in outburst (Bergeron et al. 1992; Hachisu 1986; Patterson 1984). The parameter β is a dimensionless factor of order unity that depends on the model adopted for the disruption of the disk by the stellar magnetic field (Ghosh & Lamb 1978).

For $B_* < B_{*,\text{crit}}$, the accretion disk will extend all the way to the surface of the star, for which there is good observational evidence in neutron star low mass X-ray binaries (Gilfanov et al. 2003) and in dwarf nova systems in outburst (Wheatley et al. 2003). Since the rotation rate of the star, Ω_* , is slower than the Keplerian rotation rate at the stellar surface, $\Omega_K(R_*)$, a boundary layer (BL) will exist inside of which $d\Omega/dR > 0$ and the rotation profile of the star attaches smoothly to that of the disk. If the accretion rate is high enough, it is also possible for material to spread meridionally to high latitudes forming a spreading layer (SL) (Inogamov & Sunyaev 1999; Piro & Bildsten 2004). For both a BL and a SL, the intense energy release in a localized region near the stellar surface leads to easily observable signatures such as hard spectral components, variability of emission, and so on.

A considerable amount of effort has been previously devoted to understanding the structure of well-developed, steady-state BLs, which have been evolving for long enough to establish a smooth rotation profile in their interior. An outstanding question in the study of steady-state BLs is identifying the mechanism of angular momentum transport in the layer. Several potential mechanisms have been explored over the years, among them shear instabilities (Kippenhahn & Thomas 1978), baroclinic instabilities (Fujimoto 1987; Hanawa 1987), and the Tayler-Spruit dynamo (Spruit 1999; Piro & Bildsten 2007). Despite this effort, no clear answer exists at present regarding the nature of the angular momentum transport and mixing in well-developed BLs.

1.1. Initiation of Boundary Layers

An interesting aspect of the BL problem that has received less attention in the past is the issue of BL *initiation*, i.e. the initial stage of BL formation which must occur when the accreted material first touches the surface of the star. In this case the physical setup is going to be quite different from the steady-state BL primarily because of the much larger velocity shear, justifying the study of BL initiation in the limit of an essentially discontinuous rotation profile at the interface between the star and accreting material.

Even though the initiation stage is just a transient phase in the BL evolution, one still needs to understand it to get a full picture of the BL phenomenon. Also, one need not think that the BL initiation is a unique event for every accreting object — it may, in fact, be repetitive. The most common situation in which this BL initiation is recurrent involves the dramatic increase of the mass accretion rate (due to some sort of outburst triggered by an instability) through the disk which is magnetically disrupted outside the star under normal circumstances. According to Equation (1), a sudden increase of \dot{M} by several orders of magnitude as typical for some accreting systems (e.g. dwarf novae, FU Ori outbursts, etc.) can rapidly compress the stellar magnetosphere to the point at which disk material starts touching the stellar surface and a BL starts to form.

There is good observational evidence for this kind of recurrent behavior. For instance, Livio & Pringle (1992) have argued that the observed lag in the rise time of the UV emission relative to the optical in a CV system transitioning to outburst can be explained if the disk is magnetically disrupted in quiescence but not in outburst. Thus, the hottest, innermost part of the disk is evacuated in quiescence, and UV radiation is not emitted immediately in the transition to outburst, since the empty region requires time to become filled.

FU Ori stars are another type of system in which the disk can extend all the way to the stellar surface, due to the high accretion rate - $\dot{M} \sim 10^{-4} M_{\odot} \text{yr}^{-1}$ (Kenyon et al. 1988). In these systems, the BL can puff up to become of order the stellar radius and the distinction between the boundary layer, the disk, and the star becomes blurred (Popham et al. 1993).

The goal of our present work is to make a first step towards understanding the *formation* of the BL. As in the case of a well-developed BL, the major issue for this initial stage lies in details of the angular momentum transport and mixing. However, because of the enormous shear present at the star-disk interface at this stage, it is highly likely that purely hydrodynamical shear instabilities would dominate the transport of mass and momentum rather than anything else.

For that reason, in this work we primarily focus on exploring the properties of various shear-driven instabilities under the conditions typical at the BL formation stage. First, we seek to identify a particular variety of the shear instability that most efficiently initiates mixing between the two fluids, i.e. has the fastest growth rate. Second, we examine the conditions needed for its operation, such as the density contrast between fluids, initial velocity profile, etc.

There are several physical ingredients which can potentially affect operation of shear instabilities: stratification, rotation, magnetic fields, turbulence, radiative transfer, and the supersonic nature of the flow. The latter aspect of the problem is very important and is inevitable during the BL initiation phase, when disk material rotating at the Keplerian speed comes into contact with the more slowly spinning stellar surface. The differential azimuthal velocity between the two interacting flows is then bound to be a significant fraction of the Keplerian velocity at R_* and should highly exceed the sound speed both in the disk and in the outer layers of the star.

1.2. Shear Instabilities in Compressible Fluids

The study of shear instabilities in compressible fluids is of fundamental physical significance and has received much attention in the past. Landau (1944), Hatanaka (1949), Pai (1954), Miles (1958), and Gerwin (1968) have all studied the problem in the vortex sheet approximation, where one half plane of compressible fluid moves at constant velocity over another. When the two fluids move at a low Mach number relative to each other, one finds that infinitesimal perturbations are governed by the classical Kelvin-Helmholtz (KH) dispersion relation for two incompressible fluids. However, Miles (1958) showed that above a critical Mach number, the vortex sheet becomes marginally stable to two-dimensional disturbances along the direction of the flow. This is a surprising result considering that one might have expected increasing the shear to lead to an increased growth rate for the instability rather than stabilization. Understanding the implications of this result for the momentum and mass transport in the astrophysical BLs is one of the goals of our study.

Later, Blumen et al. (1975), Ray (1982), Choudhury & Lovelace (1984) and Glatzel (1988) studied the stability of a fluid with a continuous and monotonically varying velocity profile. They found that unlike the vortex sheet, continuous velocity profiles with a supersonic velocity difference across them were unstable even at high Mach number. Glatzel (1988) showed that the instability was similar to the Papaloizou-Pringle instability which operates in hydrodynamical disks with radial boundaries (Papaloizou & Pringle 1984). Thus, for high Mach number flow in a compressible fluid, a finite thickness velocity profile exhibits fundamentally different behavior from the vortex sheet, since it can support unstable modes. Moreover, the growth rate of the unstable modes scales as $\propto 1/L$, where L is the thickness of the shear layer. Thus, the thinner the shear layer, the faster the instability operates! This is exactly the opposite of what one might have expected from the vortex sheet stability criterion and we will provide an explanation for this in §5.

Previous studies of possible instabilities inside astrophysical BLs have been primarily concerned with the sub-sonic regime when the flow can be considered as almost incompressible (Kippenhahn & Thomas 1978; Fujimoto 1988). This regime may indeed apply in well-developed BLs with smooth shear profiles, even though at the present level of knowledge one can hardly exclude the possibility of the existence of localized regions in steady-state BLs where compressibility is still important. Our primary goal here is to extend these studies into the regime of highly compressible, supersonic flows and to explore the implications for astrophysical objects. In the course of studying supersonic shear instabilities, we will sometimes also incorporate stratification in our calculations and explore the role of rotation.

The paper is organized as follows. In §2 we present our governing set of equations and describe the formalism we use to study the stability problem. Then in §3 we study the case of the compressible vortex sheet with no gravity and show that our formalism reproduces the dispersion relation obtained by previous authors (Landau 1944; Hatanaka 1949; Pai 1954; Miles 1958; Gerwin 1968). In §4, we introduce gravity as a small parameter and perform a perturbation expansion to study what influence this has on the stability of the vortex sheet. Finally, in §5 we study the stability of

a finite width shear layer with a linear velocity profile. We derive new dispersion relations for this case and test the growth rate of the fastest growing mode using the Godunov code Athena (Stone et al. 2008).

2. Formalism

Here we discuss the formalism that we use for analytic calculations throughout the paper. We adopt cylindrical coordinates (ϖ, θ, z) and for simplicity assume that all equilibrium quantities are independent of z . Thus, for our purposes gravity is given by $-g(\varpi)\hat{\varpi}$ ($g(\varpi) > 0$), and we ignore the vertical stratification of the disk. Such a setup does not allow for the baroclinic instability, which would require $d\Omega/dz \neq 0$, but it does contain the necessary ingredients for studying shear instabilities. Given our assumptions, the equation of hydrostatic equilibrium reads

$$\bar{g}(\varpi) \equiv g(\varpi) - \varpi\Omega^2(\varpi) = -\frac{1}{\rho} \frac{dP}{d\varpi}, \quad (2)$$

where $\bar{g}(\varpi)$ is the effective gravity. The equilibrium density, pressure, and sound speed are given by $\rho(\varpi)$, $P(\varpi)$, and $s(\varpi)$ respectively.

Denoting the (ϖ, θ, z) velocities by (u, v, w) , using $v = \Omega\varpi$, and assuming adiabaticity, the Euler equations in cylindrical coordinates are

$$-\frac{\partial \rho}{\partial t} = \frac{1}{\varpi} \frac{\partial}{\partial \varpi}(\rho\varpi u) + \frac{1}{\varpi} \frac{\partial}{\partial \theta}(\rho v) + \frac{\partial}{\partial z}(\rho w) \quad (3)$$

$$\frac{Du}{Dt} = -\frac{1}{\rho} \frac{\partial P}{\partial \varpi} + \frac{v^2}{\varpi} - g \quad (4)$$

$$\frac{Dv}{Dt} = -\frac{1}{\rho\varpi} \frac{\partial P}{\partial \theta} - \frac{uv}{\varpi} \quad (5)$$

$$\frac{Dw}{Dt} = -\frac{1}{\rho} \frac{\partial P}{\partial z} \quad (6)$$

$$\frac{D(P\rho^{-\gamma})}{Dt} = 0 \quad (7)$$

$$\frac{D}{Dt} \equiv \frac{\partial}{\partial t} + u \frac{\partial}{\partial \varpi} + \frac{v}{\varpi} \frac{\partial}{\partial \theta} + w \frac{\partial}{\partial z} \quad (8)$$

On top of the zeroth order equilibrium state, we consider infinitesimal two-dimensional perturbations of the form $\delta f(\varpi) \exp[i(m\theta + k_z z - \omega t)]$, where the δ denotes an Eulerian perturbation.

Starting from Equations (3)-(7), the linearized first order equations are given by

$$i\bar{\omega}\delta\rho = \frac{1}{\varpi}(\varpi\rho\delta u)' + \frac{im\rho}{\varpi}\delta v + ik_z\rho\delta w \quad (9)$$

$$i\bar{\omega}\delta u = \frac{1}{\rho}\delta P' + \frac{\bar{g}}{\rho}\delta\rho - 2\Omega\delta v \quad (10)$$

$$i\bar{\omega}\delta v = \frac{im}{\varpi\rho}\delta P + 2B\delta u \quad (11)$$

$$i\bar{\omega}\delta w = \frac{ik_z}{\rho}\delta P \quad (12)$$

$$i\bar{\omega}\delta\rho = -C_L\rho\delta u + \frac{i\bar{\omega}}{s^2}\delta P, \quad (13)$$

where $\bar{\omega} = \omega - m\Omega$ is the phase speed in the locally corotating frame, $B = (\Omega + d(\varpi\Omega)/d\varpi)/2$ is Oort's B constant, $C_L = \gamma^{-1}d\ln P/d\varpi - d\ln\rho/d\varpi$ is the Ledoux discriminant, and the primes denote differentiation with respect to ϖ . Note that in Equations (9)-(13), we have made Cowling's approximation by ignoring the first order perturbation to the gravitational potential (Cowling 1941). This means that we are taking the self-gravity of the BL to be negligible.

We can reduce the above set of linear equations to a pair of equations in δP and δu :

$$i\left(\frac{\bar{\omega}^2}{s^2} - k_z^2 - \frac{m^2}{\varpi^2}\right)\delta P = \rho\left(C_L\bar{\omega} + \frac{2Bm}{\varpi}\right)\delta u + \frac{\bar{\omega}}{\varpi}(\varpi\rho\delta u)' \quad (14)$$

$$i\rho(\bar{\omega}^2 - \bar{g}C_L - \kappa^2)\delta u = \bar{\omega}\delta P' + \frac{\bar{\omega}\bar{g}}{s^2}\delta P - \frac{2\Omega m}{\varpi}\delta P. \quad (15)$$

Here we have introduced the epicyclic frequency $\kappa^2 = 4B\Omega$.

One generally expects the BL width δ_{BL} to be small compared to the stellar radius, $\delta_{BL} \ll R_*$. Under this assumption, we show in Appendix A that Equations (14)-(15) can be simplified to the following set of equations:

$$i\left(\frac{\bar{\omega}^2}{s^2} - k_z^2 - \frac{m^2}{R_*^2}\right)\delta P = \rho\left(C_L\bar{\omega} + \frac{m}{R_*}S\right)\delta u + \bar{\omega}(\rho\delta u)' \quad (16)$$

$$i\rho(\bar{\omega}^2 - \bar{g}C_L)\delta u = \bar{\omega}\delta P' + \frac{\bar{\omega}\bar{g}}{s^2}\delta P. \quad (17)$$

The form of Equations (16) and (17) is the same as for a plane-parallel stratified shear flow (Alexakis et al. 2002). This suggests that the effects of Coriolis force and curvature are unimportant in a radially thin BL if shear instabilities provide the turbulence, and leads us to redefine the cylindrical (ϖ, θ, z) coordinate system into a Cartesian (x, y, z) system. The perturbed quantities now have the form $\delta f(x) \exp[i(k_y y + k_z z - \omega t)]$, where $k_y \equiv m/R_*$. From this it immediately follows that $\bar{\omega} = \omega - k_y V_y(x)$, where $V_y(x) = R_*\Omega(x)$ is the velocity profile. From here on, we will ignore the rotation terms, and treat the flow in the BL as a plane parallel shear flow.

From Squire's theorem for plane parallel shear flows (Fejer & Miles 1963), any three-dimensional perturbation is mathematically equivalent to a two-dimensional perturbation upon making the

transformations $k_y \rightarrow k_y / \cos \theta$, $k_z \rightarrow 0$, and $V_y \rightarrow V_y \cos \theta$, where $\cos \theta = k_y / \sqrt{k_y^2 + k_z^2}$. Thus, it is sufficient to only consider two-dimensional perturbations ($k_z = 0$) in the stability problem, and for the rest of this paper we take perturbations in the form

$$\delta f(x) \exp[i(k_y y - \omega t)]. \quad (18)$$

Assuming two-dimensional perturbations, Equations (16) and (17) become

$$i \left(\frac{\bar{\omega}^2}{s^2} - k_y^2 \right) \delta P = \rho (C_L \bar{\omega} + k_y V_y') \delta u + \bar{\omega} (\rho \delta u)' \quad (19)$$

$$i \rho (\bar{\omega}^2 - \bar{g} C_L) \delta u = \bar{\omega} \delta P' + \frac{\bar{\omega} \bar{g}}{s^2} \delta P, \quad (20)$$

where the primes now denote differentiation with respect to x . Equations (20) and (19) can be used to obtain the generalized Rayleigh equation (Appendix B.1), which using a notation similar to Alexakis et al. (2002) reads

$$\delta \phi'' + \left(k_x^2 - g \tilde{\rho} \frac{k_s + k_g}{\tilde{W}^2} - \frac{\tilde{W}''}{\tilde{W}} \right) \delta \phi = 0. \quad (21)$$

Here,

$$\delta \phi = -\delta u \sqrt{\rho} / k_x, \quad (22)$$

is a modified stream function, and for simplicity we have dropped the bar over \bar{g} , so now g denotes the effective gravity. We have also defined the quantities:

$$\tilde{W} = k_y W \sqrt{\tilde{\rho}} / i k_x \quad (23)$$

$$W = V_y - c \text{ where } c = \omega / k \text{ is the phase speed.} \quad (24)$$

$$k_x^2 = k_y^2 (W^2 / s^2 - 1) \text{ is the square of the x-component of the wavevector} \quad (25)$$

$$\text{in the absence of shear or stratification.} \quad (26)$$

$$\tilde{\rho} = \rho f^2, \text{ where } \rho \text{ is the density.} \quad (27)$$

$$f = \exp \left(\int_0^x k_g(\zeta) d\zeta \right). \quad (28)$$

$$k_g = g / s^2 \text{ is a measure of the inverse of the local scale height.} \quad (29)$$

$$k_s = \rho' / \rho \text{ is the inverse stratification length scale.} \quad (30)$$

Note that the Ledoux discriminant is given by $C_L = -(k_g + k_s)$.

The boundary conditions on $\delta \phi$ that must be satisfied at a discontinuity in the density or the velocity are that the upper and lower fluids stay in contact and that the pressure perturbation is continuous across the interface. We show explicitly in Appendix B.2 that these conditions can be

formulated as

$$\frac{\delta\phi_+}{\tilde{W}_+} = \frac{\delta\phi_-}{\tilde{W}_-} \quad (31)$$

$$\tilde{W}_+\delta\phi'_+ - \tilde{W}'_+\delta\phi_+ - \frac{g_+\tilde{\rho}_+\delta\phi_+}{\tilde{W}_+} = \tilde{W}_-\delta\phi'_- - \tilde{W}'_-\delta\phi_- - \frac{g_-\tilde{\rho}_-\delta\phi_-}{\tilde{W}_-}. \quad (32)$$

The $+/-$ signs denote evaluation of a quantity in the upper/lower fluid at the location of the interface.

3. The Vortex Sheet without Gravity

Equations (21)-(32) are fully general and apply to an arbitrary velocity profile. In particular, we can assume that the velocity varies discontinuously at some radius $x = 0$:

$$V_y(x) = \begin{cases} \bar{V}_y, & x > 0 \\ -\bar{V}_y, & x < 0, \end{cases} \quad (33)$$

where \bar{V}_y is a constant. This is known as a vortex sheet approximation. It represents the simplest possible description of the velocity variation between the two limiting values by essentially ignoring the details of the transition. Subsequently in §5, we explore a more realistic model of the velocity variation, in which the transition occurs in a region of finite radial width. We point out that the vortex sheet approximation is valid for $k_y\delta_{BL} \ll 1$. We show in Appendix C.3 that in this limit the dispersion relation for a finite width layer of constant shear reduces to the vortex sheet dispersion relation.

We assume in this section that $g = 0$, so there is no gravity, and that ρ and s are constant above and below the interface, but can be discontinuous across it. This case has already been considered by other authors in the past including Landau (1944), Hatanaka (1949), Pai (1954), Miles (1958), and Gerwin (1968). However, the results for the case without gravity will often be referenced later in the paper and serve as a verification of the formalism we developed in §2.

Using the velocity profile (33), the generalized Rayleigh equation (21) becomes

$$\delta\phi''_{\pm} + k_{x,\pm}^2\delta\phi_{\pm} = 0, \quad (34)$$

$$(35)$$

where just as in §2, the $+/-$ signs denote the upper/lower fluids respectively. Since $k_{x,\pm}$ is constant for $V_y(x)$ given by Equation (33), we have that

$$\delta\phi_{\pm} \propto e^{-ik_{x,\pm}x}. \quad (36)$$

In general, $k_{x,\pm}$ is complex, and the sign is determined by applying the appropriate boundary conditions. We discuss the boundary conditions shortly, which will also make clear the reason

for the negative sign in the exponential of Equation (36). Plugging the expressions for $\delta\phi_{\pm}$ into Equation (32) gives

$$\tilde{W}_+ k_{x,+} \delta\phi_+ = \tilde{W}_- k_{x,-} \delta\phi_-, \quad (37)$$

where we have used $\delta\phi'_{\pm} = ik_{x,\pm} \delta\phi_{\pm}$, $\tilde{\rho}_{\pm} = \rho_{\pm}$, and $\tilde{W}'_{\pm} = 0$. Using Equation (31) to substitute for $\delta\phi_-$ in terms of $\delta\phi_+$, and substituting for \tilde{W} in terms of W and ρ we have

$$\frac{k_y}{k_{x,+}} \rho_+ W_+^2 = \frac{k_y}{k_{x,-}} \rho_- W_-^2. \quad (38)$$

Introducing the density ratio $\epsilon = \rho_+/\rho_-$, the Mach number in the upper fluid $M = \bar{V}_y/s_+$, and the phase speed normalized by the sound speed in the upper fluid $\varphi = c/s_+$, we have

$$\epsilon(M - \varphi)^2 \sqrt{(M + \varphi)^2 \frac{s_+^2}{s_-^2} - 1} = (M + \varphi)^2 \sqrt{(M - \varphi)^2 - 1}. \quad (39)$$

By the definition of the sound speed, $s^2 = \gamma P/\rho$, the condition of pressure balance everywhere throughout the flow requires that $\gamma_+^{-1} \rho_+ s_+^2 = \gamma_-^{-1} \rho_- s_-^2$, where γ_+ and γ_- are the adiabatic indices above and below the interface. Assuming $\gamma_+ = \gamma_-$, we have from pressure balance that $(s_-/s_+)^2 = \rho_+/\rho_- = \epsilon$. Thus, the dispersion relation becomes:

$$\epsilon(M - \varphi)^2 \sqrt{(M + \varphi)^2 \epsilon^{-1} - 1} = (M + \varphi)^2 \sqrt{(M - \varphi)^2 - 1}. \quad (40)$$

Miles (1958) has studied Equation (40) and found that the stability criterion, i.e. that φ is purely real, is given by

$$M > M_{\text{crit}} = \frac{1}{2}(1 + \epsilon^{1/3})^{3/2}. \quad (41)$$

This shows the surprising result that infinitesimal disturbances are stabilized at high Mach number.

However, Fejer & Miles (1963) pointed out that due to Squire's theorem, it is always possible to choose an angle θ for the wavevector with respect to the flow velocity such that the projected Mach number $M \cos \theta$ is smaller than M_{crit} . Thus, even at high Mach number, the vortex sheet without gravity is still unstable to three dimensional disturbances, which are almost perpendicular to the direction of the flow; these unstable oblique modes resemble classical KH modes. However, in the astrophysical context, a thin disk has a scale height $s/\Omega \ll R_*$, and the wavelength of the oblique modes will be small relative to the disk scale height only for very small wavelengths $\lambda \ll s/\Omega$. If the BL itself has a thickness $\delta_{BL} \gtrsim s/\Omega$, the vortex sheet approximation for the oblique modes is invalid, since either the modes don't fit into a disk scale height, or the condition $\lambda \gg \delta_{BL}$ is not satisfied.

3.1. Solutions for $M \gg 1$

Since we are interested in the high Mach number limit for the initiation of the BL, we now find analytical solutions to the dispersion relation (40) for $M \gg M_{\text{crit}}$, where M_{crit} was defined in Equation (41). Squaring Equation (40), one obtains a sixth order polynomial in φ :

$$(\epsilon^2 - (M + \varphi)^2 \epsilon)(M - \varphi)^4 - (1 - (M - \varphi)^2)(M + \varphi)^4 = 0. \quad (42)$$

This polynomial has two easy to find analytic factors (Miles 1958)

$$\varphi = \left\{ -M \left(\frac{1 - \epsilon^{1/2}}{1 + \epsilon^{1/2}} \right), -M \left(\frac{1 + \epsilon^{1/2}}{1 - \epsilon^{1/2}} \right) \right\}. \quad (43)$$

We now take the limit $M \gg M_{\text{crit}}$, in which case to terms of order $\mathcal{O}(M^{-4})$, the other four solutions to the polynomial in Equation (42) are

$$\varphi = \left\{ M + 1 + \frac{\epsilon}{2(2M + 1)^2}, M - 1 - \frac{\epsilon}{2(2M - 1)^2}, \right. \\ \left. -M + \epsilon^{1/2} + \frac{\epsilon^{1/2}}{2(2M - \epsilon^{1/2})^2}, -M - \epsilon^{1/2} - \frac{\epsilon^{1/2}}{2(2M + \epsilon^{1/2})^2} \right\}. \quad (44)$$

It is easy to see that the six roots of the polynomial (42) correspond to sound waves. Starting from Equation (25) and rearranging terms we obtain

$$W^2 k_y^2 = s^2 (k_x^2 + k_y^2). \quad (45)$$

As long as k_x is real, this is the dispersion relation for a sound wave, since W^2 is the square of the phase velocity in the frame comoving with the fluid. Plugging in the six roots from Equations (43) and (44) into Equation (25), it is straightforward to verify that $k_{x,\pm}$ are indeed real for all of them. Each of the four roots in Equation (44) has a further simple interpretation. The first two correspond to sound waves that propagate almost parallel to the interface in the $+y$ and $-y$ directions in the upper fluid, whereas the second two correspond to sound waves that propagate almost parallel to the interface in the $+y$ and $-y$ directions in the lower fluid. The two roots in Equation (43) are more difficult to interpret, but the first of these corresponds to a standing wave when the two fluids have equal density (i.e. $\epsilon = 1$).

Since each of the six roots for $M \gg M_{\text{crit}}$ yields a real value for $k_{x,\pm}$, the solutions do not damp away from the interface, and we need to apply radiation boundary conditions at $x = \pm\infty$. The proper procedure is to demand that all waves are outgoing in each fluid in a frame which is subsonic with respect to the fluid (Miles 1957b), and it is convenient to work in the comoving frame of each fluid. The dimensionless phase velocity in the frame comoving with the upper fluid is $\varphi_{+,CF} = \varphi - M$, and the analogous expression for the lower fluid is $\varphi_{-,CF} = \varphi + M$.

In order to satisfy Equation (38), $k_{x,+}$ and $k_{x,-}$ must have the same sign, so we must have either $\delta\phi_{\pm} \propto e^{i(|k_{x,\pm}|x-\omega t)}$ or $\delta\phi_{\pm} \propto e^{i(-|k_{x,\pm}|x-\omega t)}$. Moreover, since $k_{x,+}$ and $k_{x,-}$ have the same sign, it is clear that $\varphi_{+,CF}$ and $\varphi_{-,CF}$ must have the opposite sign to yield outgoing waves in the comoving frames of each of the two fluids. Only three of the six roots found above satisfy this condition:

$$\varphi_l = -M + \epsilon^{1/2} + \frac{\epsilon^{1/2}}{2(2M - \epsilon^{1/2})^2} \quad (46)$$

$$\varphi_m = -M \left(\frac{1 - \epsilon^{1/2}}{1 + \epsilon^{1/2}} \right) \quad (47)$$

$$\varphi_u = M - 1 - \frac{\epsilon}{2(2M - 1)^2}. \quad (48)$$

We will refer to these three roots as the lower, middle, and upper branches, respectively. Furthermore, it is straightforward to check that the solutions which yield outgoing waves in both the upper and lower fluids have $\delta\phi_{\pm} \propto e^{i(-|k_{x,\pm}|x-\omega t)}$, so $k_{x,\pm}$ are positive given our definition (36).

3.2. Dispersion Relation in the General Case

We now relax the assumption of $M \gg 1$ and numerically solve the dispersion relation (40) at arbitrary Mach number for $\epsilon = 1$ (Figure 1a) and $\epsilon = .01$ (Figure 1b). At the critical Mach number given by Equation (41), the upper and lower branches merge together in the real plane and bifurcate in the complex plane. These bifurcated solutions turn into the two incompressible KH modes for $M \ll M_{\text{crit}}$. Unlike, the lower and upper branches, the middle branch has no incompressible analog and ceases to be a viable physical solution below a critical Mach number

$$2M_m = 1 + \epsilon^{\frac{1}{2}}. \quad (49)$$

The reason for this is that below $M = M_m$, $k_{x,\pm}$ switches from real to imaginary and the boundary conditions for the middle branch at $x = \pm\infty$ can no longer be satisfied.

4. The Isothermal Vortex Sheet with Gravity

We now go beyond the simplifying assumption of no gravity used in §3 and consider the case where g is non-zero and constant. We shall shortly assume an isothermal equation of state, but for now we consider the more general polytropic equation of state of the form $P = K_{\pm}\rho^n$ in each of the two fluids. For any equation of state of this form, we have

$$k_g = \frac{g}{s^2} = -\frac{\frac{\partial P}{\partial \rho} \frac{d\rho}{dr}}{\gamma P} = -\frac{n}{\gamma} \frac{d \ln \rho}{dr} = -\frac{n}{\gamma} k_s, \quad (50)$$

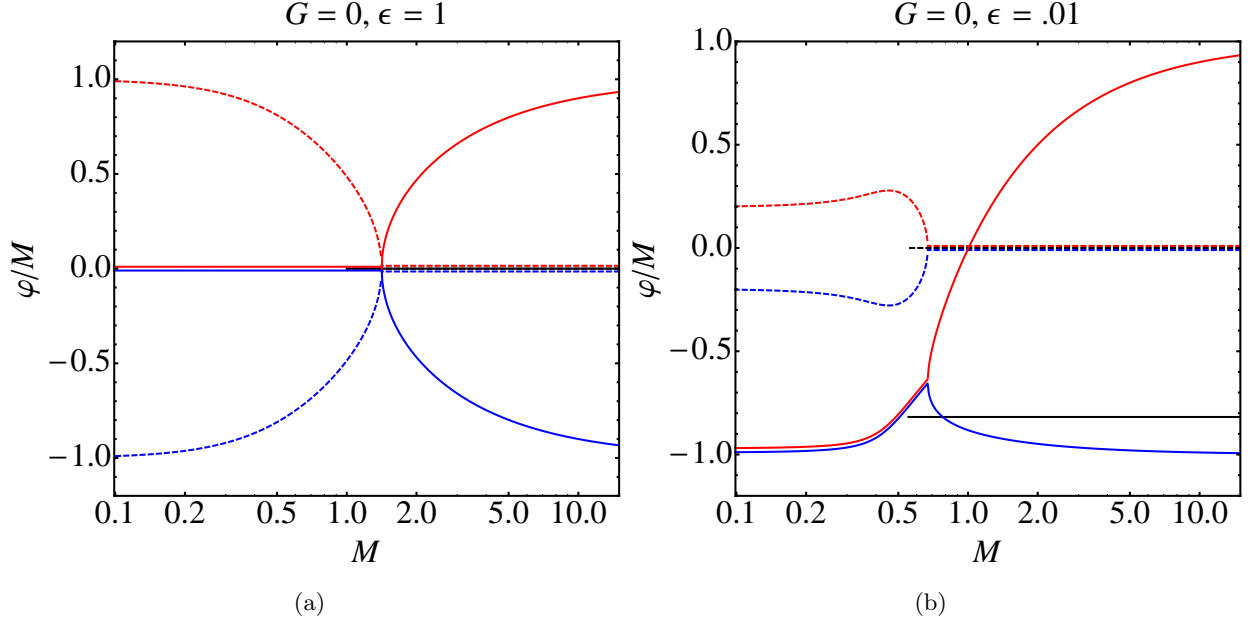


Fig. 1.— The dispersion relation φ/M as a function M for $\epsilon = 1$ and $\epsilon = .01$. The solid and dashed curves give the real and imaginary components respectively. The blue, black, and red curves correspond to the lower, middle, and upper branches respectively. The red and blue curves have been slightly offset vertically so they do not overlap.

which means $k_s + k_g = (1 - \gamma/n)k_g$. If $n = \gamma$, corresponding to the case of an adiabatic atmosphere, the second term in parentheses in Equation (21) drops out, but then the third term becomes difficult to treat analytically. However, for an isothermal atmosphere ($n = 1$) the sound speed is constant, and both the second and third terms in Equation (21) reduce to a tractable form. Since we are only interested in the gross, qualitative properties of the flow, we assume both fluids are isothermally stratified, since this assumption significantly simplifies the analytical treatment.

For $n = 1$, the second term in Equation (21) becomes

$$-g\tilde{\rho}\frac{k_s + k_g}{\tilde{W}^2} = gk_g(1 - \gamma)\frac{k_x^2}{k_y^2\tilde{W}^2} \quad (51)$$

We now again assume a vortex sheet velocity profile (Equation (33)), in which case for $n = 1$, the third term in Equation (21) is given by

$$\frac{\tilde{W}''}{\tilde{W}} = \frac{(\sqrt{\tilde{\rho}})''}{\sqrt{\tilde{\rho}}} = \left(\frac{2 - \gamma}{2}k_g\right)^2 \quad (52)$$

Putting Equations (51) and (52) into Equation (21), we have

$$\begin{aligned} \delta\phi'' + \tilde{k}_x^2\delta\phi &= 0, \\ \tilde{k}_x^2 &\equiv \left[k_x^2 \left(1 - (\gamma - 1) \left(\frac{k_g}{k_y} \right)^2 \left(\frac{s}{\tilde{W}} \right)^2 \right) - \left(\frac{2 - \gamma}{2} k_g \right)^2 \right]. \end{aligned} \quad (53)$$

The perturbation is then given as

$$\delta\phi_{\pm} \propto e^{-i\tilde{k}_{x,\pm}x}. \quad (54)$$

We now comment on the terms present in Equation (53). In the absence of gravity, $k_g = 0$, and we simply have $\tilde{k}_x = k_x$. If $k_g \neq 0$, then the second term on the right hand side of Equation (53) can be written in a more familiar form as

$$(\gamma - 1) \left(\frac{k_g}{k_y}\right)^2 \left(\frac{s}{\tilde{W}}\right)^2 = \left(\frac{N}{\omega - k_y V_y}\right)^2, \quad (55)$$

where

$$N^2 = \frac{(\gamma - 1)g^2}{s^2} \quad (56)$$

is the Brunt-Väisälä frequency. Thus, the second term on the right hand side of Equation (53) provides a lower frequency cutoff for sound waves at the Brunt-Väisälä frequency. The last term in Equation (53) arises because we have *not* made the short wavelength approximation $k_x \gg k_g$.

Now, we use the boundary conditions (31) and (32) to determine the dispersion relation. Substituting $\delta\phi'_{\pm} = -i\tilde{k}_{x,\pm}\delta\phi_{\pm}$, and $\tilde{W}'_{\pm} = (2 - \gamma)k_{g,\pm}\tilde{W}_{\pm}/2$ into the condition (32), we have

$$- \left[i\tilde{k}_{x,+} + \left(\frac{2 - \gamma}{2} \frac{g}{s_+^2} \right) \right] \tilde{W}_+ \delta\phi_+ - \frac{g\tilde{\rho}_+ \delta\phi_+}{\tilde{W}_+} = - \left[i\tilde{k}_{x,-} + \left(\frac{2 - \gamma}{2} \frac{g}{s_-^2} \right) \right] \tilde{W}_- \delta\phi_- - \frac{g\tilde{\rho}_- \delta\phi_-}{\tilde{W}_-}. \quad (57)$$

Next, using the second boundary condition (31) to substitute for $\delta\phi_-$ in terms of $\delta\phi_+$, and using the fact that $\tilde{\rho}_{\pm} = \rho_{\pm}$ at the interface, we have

$$- \left[i\tilde{k}_{x,+} + \left(\frac{2 - \gamma}{2} \frac{g}{s_+^2} \right) \right] \tilde{W}_+^2 - g\rho_+ = - \left[i\tilde{k}_{x,-} + \left(\frac{2 - \gamma}{2} \frac{g}{s_-^2} \right) \right] \tilde{W}_-^2 - g\rho_-. \quad (58)$$

We now introduce the dimensionless gravity parameter

$$G = \frac{g}{k_y s_+^2}, \quad (59)$$

which is closely related to the ratio of the wavelength to the pressure scale height, h_s . Thus, $G \sim 1$ when $k_y h_{s,+} \sim 1$, and $G\epsilon^{-1} \sim 1$ when $k_y h_{s,-} \sim 1$. Using $\epsilon = \rho_+/\rho_- = s_-^2/s_+^2$, and performing some algebra, we have

$$\left[i\frac{\tilde{k}_{x,+}}{k_y} + \left(\frac{2 - \gamma}{2} G \right) \right] \left(\frac{k_y}{\tilde{k}_{x,+}} \right)^2 \left(\frac{W_+}{s_+} \right)^2 \epsilon + G(1 - \epsilon) = \left[i\frac{\tilde{k}_{x,-}}{k_y} + \left(\frac{2 - \gamma}{2} G\epsilon^{-1} \right) \right] \left(\frac{k_y}{\tilde{k}_{x,-}} \right)^2 \left(\frac{W_-}{s_+} \right)^2. \quad (60)$$

Setting $G = 0$ it is clear that we recover the vortex sheet dispersion relation in the absence of gravity (Equation (38)).

We now check Equation (60) by showing that it reproduces the well-known incompressible KH dispersion relations in the limit $M \ll M_{\text{crit}}$, before going on to treat the case of the supersonic vortex sheet with gravity.

4.1. Highly Subsonic Vortex Sheet with Gravity

We assume that $\bar{V}/s_{\pm} \ll 1$, which immediately implies $M \ll M_{\text{crit}}$, and we also assume $G \ll 1$ and $G\epsilon^{-1} \ll 1$, which means that the wavelength of the perturbation is much smaller than the scale height in both the upper and lower fluids ($k_{g,\pm}/k_y \ll 1$). Next, we eliminate sound wave modes by assuming $\varphi \ll 1$ (phase velocity much lower than sound velocity in upper fluid) and $\varphi\epsilon^{-1/2} \ll 1$ (phase velocity much lower than sound velocity in lower fluid). According to Equation (53), this means $k_x = \pm ik_y$, and given our definition for $\delta\phi_{\pm}$ in Equation (54), we must chose the minus sign in the upper fluid and the plus sign in the lower fluid to give vanishing solutions at $x = \pm\infty$. Equation (60) then yields

$$-\epsilon \left(\frac{\omega}{k_y} - \bar{V}_y \right)^2 \sqrt{1 - \frac{(\gamma - 1)G^2}{(M - \varphi)^2} + \frac{g}{k_y}(1 - \epsilon)} = \left(\frac{\omega}{k_y} + \bar{V}_y \right)^2 \sqrt{1 - \frac{(\gamma - 1)G^2\epsilon^{-1}}{(M + \varphi)^2}}. \quad (61)$$

Next, we note that $(\gamma - 1)G^2/(M - \varphi)^2 = N_+^2/(\omega - k_y\bar{V}_y)^2$ and that $(\gamma - 1)G^2\epsilon^{-1}/(M + \varphi)^2 = N_-^2/(\omega + k_y\bar{V}_y)^2$, where N is the Brunt-Väisälä frequency for an isothermal atmosphere and was given in Equation (56). We expect $|\omega \pm k_y\bar{V}_y| \gtrsim \sqrt{gk}$, which is the characteristic frequency of surface gravity waves. Since $N_{\pm} \sim \sqrt{gk_{g,\pm}}$, and we have already assumed $k_{g,\pm}/k_y \ll 1$, it follows that $N_{\pm} \ll |\omega \mp k_y\bar{V}_y|$. Consequently, Equation (61) reduces to

$$-\epsilon \left(\frac{\omega}{k_y} - \bar{V}_y \right)^2 + \frac{g}{k_y}(1 - \epsilon) = \left(\frac{\omega}{k_y} + \bar{V}_y \right)^2, \quad (62)$$

which is the well known KH dispersion relation for an incompressible fluid in the presence of gravity.

4.2. The Weak Gravity Limit at High Mach Number

As mentioned before in §3.1, Miles (1958) has demonstrated that in the absence of gravity, the vortex sheet is stable above a critical Mach number given by Equation (41). We now address the question of whether the system still remains stable when $G \neq 0$.

To answer this question, we will use our general dispersion relation (60) in which we will additionally assume $M \gg M_{\text{crit}}$, since this assumption significantly simplifies the algebra. Since we have already obtained solutions for the case $G = 0$ and $M \gg M_{\text{crit}}$ (§3.1), we proceed by considering gravity as a perturbation. We consider wavelengths that are much smaller than the pressure scale height and ask what happens in the limit $G \rightarrow 0$. In our analysis, we will assume that the density ratio $\epsilon \leq 1$, so that the system is stable to the Rayleigh-Taylor instability.

Because the introduction of gravity makes the upper and lower fluids stratified, some care should be taken when determining which solutions are physical and which are not. Miles (1957b) has shown that for $G = 0$, the three supersonic KH modes can be understood in terms of sound waves emitted from the interface between the two fluids. This interpretation is useful as well for the case with gravity and leads to a couple of insights. First, the amplitude of sound waves is not constant

as they propagate through a stratified medium. Rather, to conserve energy, waves propagating upward (to lower densities) must increase in amplitude, and those propagating downward (to higher densities) must decrease in amplitude. Second, since the sound waves are emitted from the interface, if ω has an imaginary component, then the amplitude of the emitted waves changes with time. Thus, if $\Im[\omega] > 0$, and there is an instability, then the amplitude of the waves will decay with distance from the interface, since the waves emitted in the past had lower amplitude. Conversely if $\Im[\omega] < 0$ and the perturbation is damping in time, then the amplitude of the emitted waves will increase with distance from the interface, since the waves emitted in the past had a larger amplitude. Both of these effects mean that the amplitude of the waves can blow up as we move away from the interface. Thus, we take as physical those solutions which yield outgoing waves (away from the interface) in both the upper and lower fluids, even if these solutions diverge as $x \rightarrow \pm\infty$. For the limit $G \rightarrow 0$, this means that the physical solutions are still the lower, middle, and upper branches but now modified by the presence of a weak gravitational field.

We note here that although the dispersion relation (60) is valid for all values of G and not just for small G , the simple picture of outgoing sound waves in the upper and lower fluids is only valid for $G \rightarrow 0$. From a physical point of view, this can be attributed to the following fact. Sound waves (p-modes) traveling in a stratified atmosphere have a frequency cutoff at $\omega^2 = N^2$ below which propagation is not possible. Given our definitions of k_y and \tilde{k}_x , the frequency of a sound wave in the frame comoving with the fluid is $\omega^2 \sim (k_y^2 + \tilde{k}_x^2)s^2$. Substituting $N^2 \sim \omega^2$ and using the definition of N^2 (Equation (56)) yields $G^2 < (\gamma - 1)^{-1}(1 + (|\tilde{k}_x|/k_y)^2)$ for sound waves to propagate. If this condition is not fulfilled, then the picture of outgoing sound waves is invalid, and the boundary conditions need to be formulated in a different way, which is beyond the scope of the present work.

4.2.1. The Lower Branch

We begin by considering how the lower wave is modified in the limit $G \rightarrow 0$ and $M \gg M_{\text{crit}}$. If $G = 0$ exactly, then $\tilde{k}_x = k_x$, and in the limit $G \rightarrow 0$ we have $\tilde{k}_x = k_x(1 + \mathcal{O}(G^2))$. Keeping terms only to first order in G , Equation (60) becomes

$$\left[i \frac{k_{x,+}}{k_y} + \left(\frac{2-\gamma}{2} G \right) \right] \left(\frac{k_y}{k_{x,+}} \right)^2 \left(\frac{W_+}{s_+} \right)^2 \epsilon + G(1-\epsilon) = \left[i \frac{k_{x,-}}{k_y} + \left(\frac{2-\gamma}{2} G \epsilon^{-1} \right) \right] \left(\frac{k_y}{k_{x,-}} \right)^2 \left(\frac{W_-}{s_+} \right)^2. \quad (63)$$

Writing this out explicitly in terms of M and φ gives

$$\frac{i(M-\varphi)^2\epsilon}{\sqrt{(M-\varphi)^2-1}} - \frac{i(M+\varphi)^2}{\sqrt{(M+\varphi)^2\epsilon^{-1}-1}} + G(1-\epsilon) = \frac{2-\gamma}{2} G \left(\frac{(M+\varphi)^2\epsilon^{-1}}{(M+\varphi)^2\epsilon^{-1}-1} - \frac{(M-\varphi)^2\epsilon}{(M-\varphi)^2-1} \right). \quad (64)$$

Next, we assume that gravity only weakly affects the dispersion relation and make the perturbative expansion

$$\varphi = \varphi_0 + \varphi_1, \quad |\varphi_1|/|\varphi_0| \ll 1, \quad (65)$$

where φ_0 is the solution for $G = 0$ and $M \gg M_{\text{crit}}$.

For the lower branch, we can use Equation (46) for φ_0 , and in the limit $M \gg M_{\text{crit}}$ we have

$$\varphi_0 \approx -M + \epsilon^{1/2} \quad (66)$$

$$\frac{k_{x,+}}{k_y} = \sqrt{(M - \varphi_0)^2 - 1} \approx 2M - \epsilon^{1/2} \quad (67)$$

$$\frac{k_{x,-}}{k_y} = \sqrt{(M + \varphi_0)^2 \epsilon^{-1} - 1} \approx \frac{1}{2M - \epsilon^{1/2}}. \quad (68)$$

Defining

$$M_l \equiv 2M - \epsilon^{1/2}, \quad (69)$$

Equation (64) becomes

$$\frac{i(M_l - \varphi_1)^2 \epsilon}{\sqrt{(M_l - \varphi_1)^2 - 1}} - \frac{i(\epsilon^{1/2} + \varphi_1)^2}{\sqrt{(\epsilon^{1/2} + \varphi_1)^2 \epsilon^{-1} - 1}} + G(1 - \epsilon) = \frac{2 - \gamma}{2} G \left(\frac{(\epsilon^{1/2} + \varphi_1)^2 \epsilon^{-1}}{(\epsilon^{1/2} + \varphi_1)^2 \epsilon^{-1} - 1} - \frac{(M_l - \varphi_1)^2 \epsilon}{(M_l - \varphi_1)^2 - 1} \right). \quad (70)$$

It will turn out (Equation (72)) that φ_1 is proportional to G , so working to first order in G is equivalent to working to first order in φ_1 . Equation (70) then simplifies to

$$i(M_l - \varphi_1) \epsilon - \frac{iM_l \epsilon (1 + 2\epsilon^{-1/2} \varphi_1)}{1 + M_l^2 \epsilon^{-1/2} \varphi_1} + G(1 - \epsilon) = \frac{2 - \gamma}{2} G \left(M_l^2 \frac{1 + 2\epsilon^{-1/2} \varphi_1}{1 + 2M_l^2 \epsilon^{-1/2} \varphi_1} - \epsilon \right). \quad (71)$$

Assuming $|M_l^2 \epsilon^{-1/2} \varphi_1| \ll 1$, and keeping terms to leading order in M_l , we can solve for φ_1 in terms of G .

$$\varphi_{1,l} \approx -\frac{2 - \gamma}{2} \frac{G}{M_l \epsilon^{1/2}} i. \quad (72)$$

We immediately see two things from Equation (72). First, φ_1 is purely imaginary, and second, if $\gamma < 2$, φ_1 is negative and the perturbation damps, whereas if $\gamma > 2$, φ_1 is positive and the perturbation grows. For realistic equations of state, $\gamma \leq 5/3$, so the lower wave always damps.

4.2.2. The Middle and Upper Branches

We can find an approximate solution for φ_1 in the limit $G \rightarrow 0$ and $M \gg M_{\text{crit}}$ for the middle and upper branches in much the same manner as for the lower branch. The first order correction for the middle branch is

$$\varphi_{1,m} = -\frac{\gamma}{2} \frac{G(1 - \epsilon^{1/2})}{\epsilon^{1/2}} i, \quad (73)$$

and for the upper branch is

$$\varphi_{1,u} \approx \frac{2 - \gamma}{2} \frac{G \epsilon^{1/2}}{2M - 1} i. \quad (74)$$

Just as in the case of the lower branch, φ_1 is purely imaginary for both the middle and upper branches. We see that φ_1 is negative for the middle branch if $\epsilon < 1$. However, for the upper branch if $\gamma < 2$, φ_1 is positive and if $\gamma > 2$, φ_1 is negative. This is opposite from the lower branch meaning that for any $\gamma \neq 2$ in the limit $M \gg 1$, one of the two branches is always unstable and the other one is damped. For a realistic equation of state, $\gamma \leq 5/3$ so the upper branch is the unstable one, and the lower branch damps.

4.2.3. Numerical Verification

We verify Equations (72), (73), and (74) numerically by solving the fully general dispersion relation (60) and comparing $\Im(\varphi)$ with our analytical estimate for the parameters $M = 5$, $\epsilon = .5$, and $\gamma = 5/3$. We plot $\Im(\varphi)$ vs. G in for both our analytical solutions (solid lines) and the ones obtained numerically (dashed lines) in Figure 2. The analytical solution converges to the numerical one in the limit $G \rightarrow 0$.

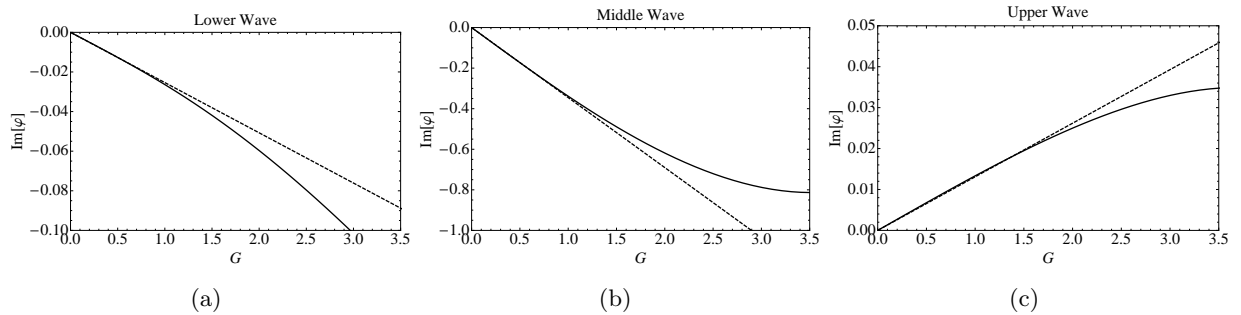


Fig. 2.— Plots of $\Im(\varphi)$ vs. G for the lower (a), middle (b), and upper (c) branches respectively, using $M = 5$, $\epsilon = .5$, $\gamma = 5/3$. The solid curves show the numerical solution obtained by solving Equation (60) and the dashed curves correspond to the approximate solutions from Equations (72), (73), and (74).

5. Sonic Instabilities in a Finite Width Layer of Constant Shear

The calculations presented in §3,4 were performed for the velocity profile (33) featuring a discontinuity at some radius. We now consider a more complicated (and more realistic at later stages of the BL evolution) initial setup in which the velocity between the two fluids varies *continuously* within a narrow shear layer. Unlike the vortex sheet, the finite width shear layer without gravity is known to be unstable at high Mach number (Glatzel 1988; Choudhury & Lovelace 1984; Ray 1982), and in this case the growth rate of the instability scales inversely with the width of the shear layer and in proportion to the shear, $S \sim \Omega_K R_* / \delta_{BL}$.

In the following, we extend some of the findings of Glatzel (1988) to study sonic instabilities

in a finite width shear layer without gravity and apply them to the problem of the BL initiation. The setup we consider has the velocity profile

$$V(x) = \begin{cases} \bar{V}, & x > \delta_{BL}, \\ \bar{V}x/\delta_{BL}, & -\delta_{BL} \leq x \leq \delta_{BL}, \\ -\bar{V}, & x < -\delta_{BL} \end{cases} \quad (75)$$

and the density profile

$$\rho(x) = \begin{cases} \rho_+, & x > -\delta_{BL} \\ \rho_-, & x < -\delta_{BL} \end{cases} \quad (76)$$

Pressure equilibrium again requires that $\rho_+ s_+^2 = \rho_- s_-^2$, which sets the sound speed everywhere in the flow, and as before we have $\epsilon = \rho_+/\rho_-$ and $M = \bar{V}/s_+$.

Although we only consider a linearly varying velocity profile in the shear layer, Ray (1982) and Choudhury & Lovelace (1984) have found that different shear profiles are qualitatively similar. Thus, we consider a constant shear to be representative of more general shear profiles.

5.1. Dispersion Relation

We now study the dispersion relation of the finite width shear layer. In applying the dispersion relation to the initiation of the BL, we are most interested in the growth rate of the fastest growing mode for $M \gg 1$. Glatzel (1988) has already obtained the dispersion relation for the case $\epsilon = 1$, and using his techniques, we derive the dispersion relation for the case of arbitrary ϵ in Appendix C. We also show in Appendix C.3 that the dispersion relation for a finite width shear layer reduces to the dispersion relation for a vortex sheet in the limit $k_y \rightarrow 0$ at constant δ_{BL} .

In Figure 3, we plot the dispersion relation (C20) as a function of wavenumber for the parameters $M = 5$ and $\epsilon = 1$, $\epsilon = .25$, $\epsilon = .1$, $\epsilon = .01$, and $\epsilon = 0$. The $\epsilon = 0$ case is equivalent to having a hard reflecting boundary at $x = -\delta_{BL}$. The modes depicted are the ones that converge to the upper and lower branches from §3 in the vortex sheet limit ($k_y \delta_{BL} \ll 1$). For $\epsilon < 1$, the upper branch always has a larger growth rate than the lower branch, and both the upper and lower branches have the same growth rate for $\epsilon = 1$. In the $\epsilon = 1$ case, we can identify the upper and lower branches as the $n_{\pm} = 0$ decoupled modes in §5.4 of Glatzel (1988). In addition to the upper and lower waves, Glatzel (1988) has shown that there is an infinite spectrum of damped modes, but we do not consider these here, since we are interested in determining the growth rate of the fastest growing mode.

We now revisit the seemingly paradoxical statement that the vortex sheet is stable to two dimensional disturbances along the flow direction above a critical Mach number; yet at the same time, the growth rate of the fastest growing mode scales with δ_{BL}^{-1} , which implies that the thinner the shear layer, the faster the instability proceeds. The key to resolving this apparent controversy

is to consider a mode having $k_y \delta_{BL} \ll 1$. Its growth rate is diminished if we decrease δ_{BL} while keeping k_y constant for $M > M_{\text{crit}}$ and becomes vanishingly small if we take the limit $\delta_{BL} \rightarrow 0$. This can be seen from the dying left hand tail of the curve in Figure 3b, and keeping k_y constant, while decreasing δ_{BL} we move leftward along the tail. This means $\Im[\omega]$ becomes smaller, since $\varphi = \omega/k_y s_+$ is directly proportional to ω for constant k_y even as we decrease δ_{BL} . We next point out that the curve in Figure 3c remains unchanged in shape or amplitude as we decrease δ_{BL} , keeping $k_y \delta_{BL}$ constant. Consequently, the value of k_y for which the maximum in $\Im[\omega]$ occurs $k_{y,\text{max}} \propto \delta_{BL}^{-1}$ and likewise $\max[\Im[\omega]] \propto \delta_{BL}^{-1}$. Thus, as δ_{BL} is decreased, the instability shifts to shorter wavelengths and becomes more rapid, while at the same time, modes having $k_y \delta_{BL} \ll 1$ are stabilized for a given value of k_y . Since any real shear layer is likely to have a nonzero width, one may therefore remark that taking the vortex sheet limit for $M \gg M_{\text{crit}}$ masks the instability.

5.2. Numerical Verification

To independently verify our dispersion relation (C20), we ran direct hydrodynamical simulations of shear layers using the Godunov code Athena (Stone et al. 2008) and compared the growth rate of the fastest growing mode predicted by our dispersion relation to that obtained in the simulations. We initialized a flow along the y -direction using the setup described by Equations (75), and for all of the simulations we used $\gamma = 5/3$, $\delta_{BL} = 1$ for the half width of the shear layer, and periodic boundary conditions in the y -direction; Table 1 summarizes the simulation specific parameters. To seed the instability, we initialized random perturbations to v_x of magnitude 10^{-6} in the region $x > -1$. We found that for the $M = 5$ runs, we needed a high resolution in the x -direction to get converged estimates for the growth rates. Figure 4 shows $\rho v_x^2/2$ averaged over box as a function of time. The solid lines show simulation results, and the dashed lines show the predictions from considering the fastest growing mode for the upper branch, using the dispersion relation (C20). There is good agreement between the two, especially for the limiting cases of $\epsilon = 0$ and $\epsilon = 1$.

Label	M	ϵ	x -range	y -range	$N_x \times N_y$	(BC- $x1$, BC- $x2$)
A	5	1	(-4,4)	(-16,16)	8192 \times 8192	(outflow, outflow)
B	5	.25	(-4,4)	(-16,16)	8192 \times 8192	(outflow, outflow)
C	5	.1	(-4,4)	(-16,16)	8192 \times 8192	(outflow, outflow)
D	5	0	(-1,4)	(-16,16)	2048 \times 2048	(reflecting, outflow)
E	.05	1	(-4,4)	(-8,8)	512 \times 512	(reflecting, reflecting)

Table 1: Parameters for the simulations with Athena. M – Mach number, ϵ – density ratio, x, y -range – box size in x, y -direction, $N_x \times N_y$ – number of cells in x, y -direction, (BC- $x1$, BC- $x2$) – lower and upper boundary conditions in x direction.

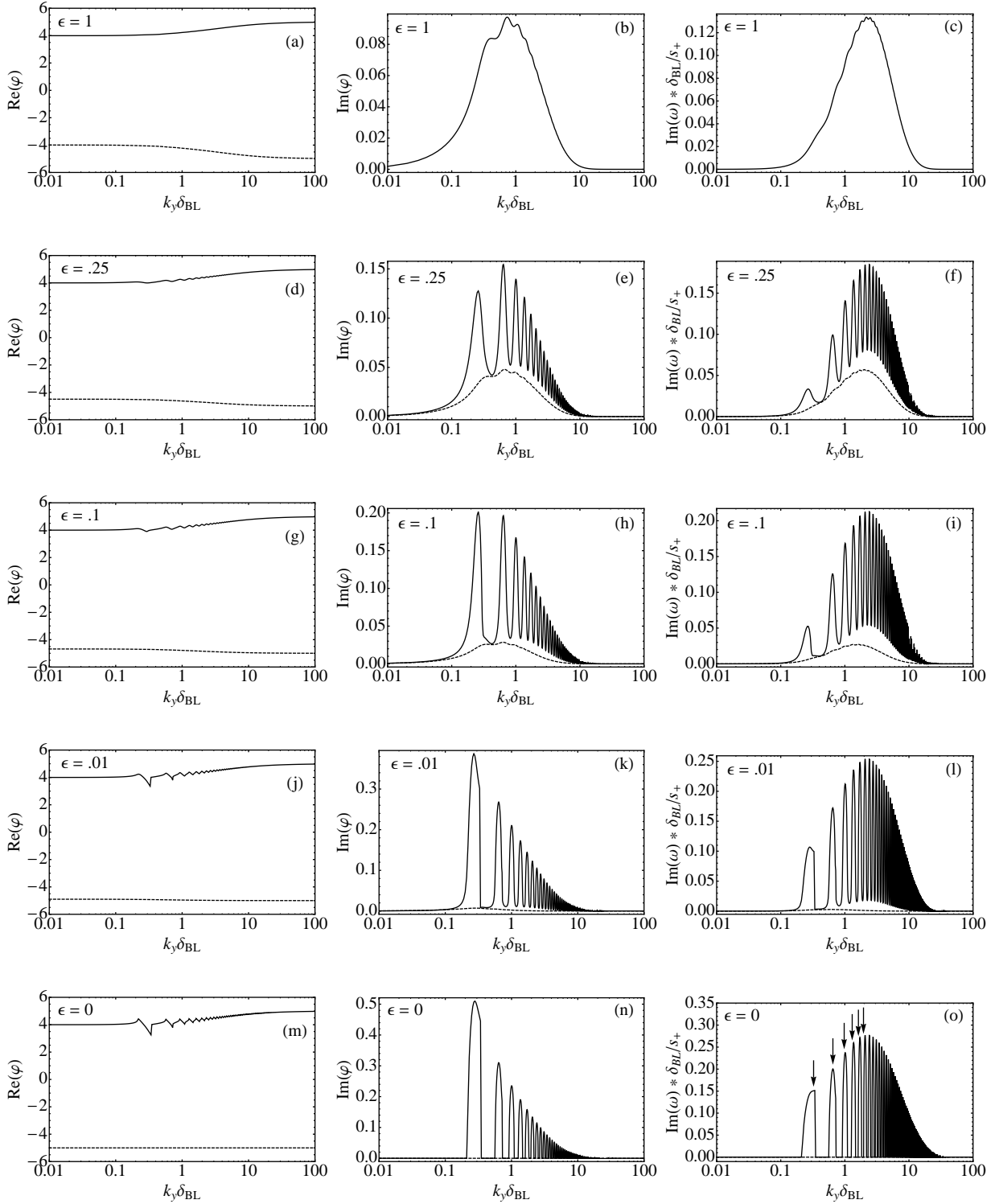


Fig. 3.— Dispersion relations for $M = 5$ and a finite width shear layer. The top row is for $\epsilon = 1$, the second row for $\epsilon = .25$, the third row for $\epsilon = .1$, the fourth row for $\epsilon = .01$, and the bottom row for $\epsilon = 0$. The first column shows the real part of φ , the second the imaginary part of φ and the third the imaginary part of ω . The solid line corresponds to the upper branch and the dashed line to the lower branch. In the top row, the upper and lower branches have the same growth rate. The arrows in panel (o) show the wavenumbers corresponding to trapped wavenumbers (§5.3).

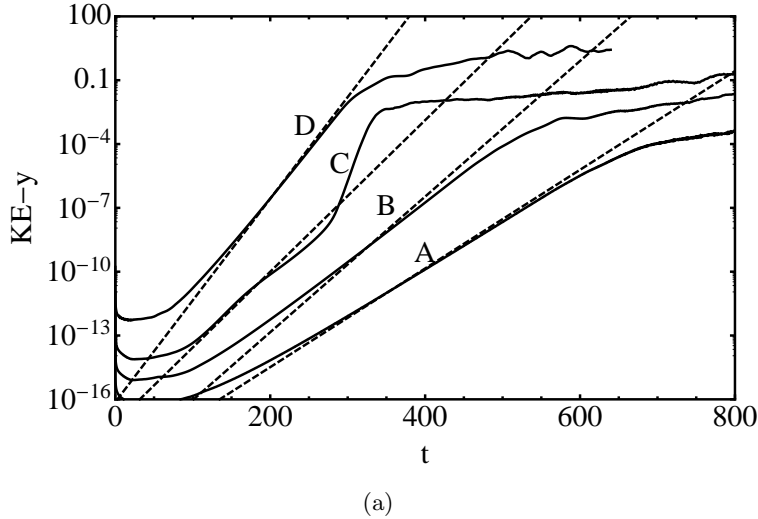


Fig. 4.— Comparison of the analytically derived growth rates (given by the slopes of the dashed lines) to the ones obtained using Athena (solid lines). The curves A, B, C, D correspond to $\epsilon = 1, .25, .1,$ and 0 , respectively (see text for further simulation details) and have been offset vertically for clarity.

5.3. Physical Intuition

Panels, (a), (b), and (c) of Figure 5 show the spatial structure of v_x for simulations A, E & D during the linear stage of the instability. The fastest growing modes in these three cases are very different, illustrating the different instability mechanisms which operate for the $M \gg M_{\text{crit}}$ vs. $M \ll M_{\text{crit}}$ cases and also for $\epsilon = 1$ vs. $\epsilon = 0$. The case $M \ll M_{\text{crit}}$, in panel (b) has been extensively studied (e.g. (Vallis 2006)), so we will not consider it here..

For the $M \gg M_{\text{crit}}$ case with $\epsilon = 1$, the instability is caused by a *radiation mechanism*. This mechanism has already been discussed by Glatzel (1988), so we only mention it here briefly. Each mode of the dispersion relation can be associated with a pseudo-energy that is conserved. If a mode has a negative pseudo-energy, then radiation of energy away from the boundary layer region will cause the pseudo-energy to become even more negative, amplifying the mode and leading to instability. The radiation mechanism is responsible for the smooth, broad hump in panels (b) and (c) of Figure 3.

For the case of $M \gg M_{\text{crit}}$ and $\epsilon = 0$, the instability mechanism is quite different. Rather than a broad hump, panels (n) and (o) of Figure 3 exhibit sharp localized peaks. The physical cause of these peaks is due to over-reflection of modes that become trapped between the lower boundary and the critical layer. Thus, we shall call this the *over-reflection mechanism*.

The over-reflection mechanism is discussed in Narayan et al. (1987), who considered a rotating shear layer adjacent to a reflecting wall. They explained the instability in the $\epsilon = 0$ case in terms

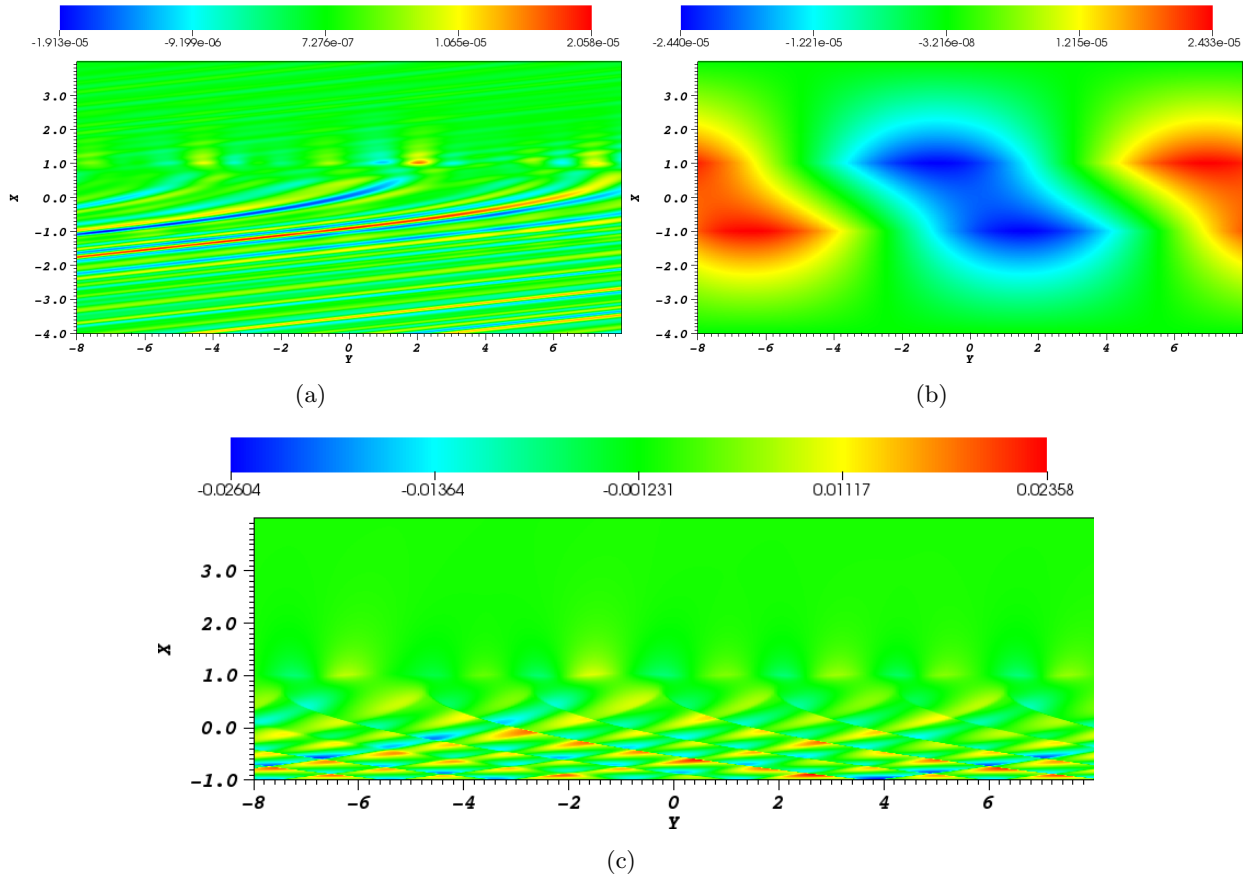


Fig. 5.— Panels (a), (b), and (c) show v_x during the linear stage of the instability for simulations A, E, & D respectively and have been rotated by 90 degrees.

of the leaking of action density past the corotation radius, which is the analog of the critical layer for a rotating system. Like the pseudo-energy of Glatzel (1988), the action density is a conserved quantity, and instability occurs because a wavemode that is trapped between the critical layer and the wall has a negative action density, whereas positive action leaks out past the critical layer. As a result, the amplitude of the trapped wavemode becomes even more negative and grows with time. Put in this way, it is clear that the over-reflection and radiation mechanisms are related. However, they lead to a very different structure for the dispersion relation, as evidenced by panels (n) and (o) vs. panels (b) and (c) of Figure 3. Thus, we prefer to regard them as separate mechanisms, but point out that in both cases, instability is ultimately caused by radiation emitted from the boundary layer region.

We now elucidate some of the properties of the modes that are trapped between the critical layer and the lower reflecting boundary using a simple model. Consider a sonic mode that is trapped between the lower boundary and the critical layer. If the mode has a well-defined phase velocity, then by performing a velocity boost one can transform into a frame in which the wavefronts are

stationary. Let us work in this frame, since it makes the explanations more clear. In order for the wavefronts to be stationary, the equation for a wavefront is

$$\frac{dy}{dx} = \pm \sqrt{\mathcal{M}(x)^2 - 1}. \quad (77)$$

Here, $\mathcal{M}(x)$ is the Mach number as a function of x , and the positive sign is for waves propagating in the $-x$ direction, while the negative sign is for waves propagating in the $+x$ direction. Equation (77) is obtained from the fact that the wavefront propagates at the speed of sound, and in order for it to be stationary, the angle that the wavefront forms with the y -direction obeys $\sin(\theta) = 1/\mathcal{M}(x)$.

Consider now the upper branch from §3.1, for which the critical layer is at $x_c = \delta_{BL}(M-1)/M$. At the critical layer, we set $dy/dx = 0$, which is just to say that an upward traveling sound wave is reflected there. It immediately follows that inside the region of shear

$$\mathcal{M}(x) = -M \left(1 - \frac{x}{\delta_{BL}} \right), \quad -\delta_{BL} \leq x \leq \delta_{BL}. \quad (78)$$

$$(79)$$

Thus, the frame in which sound waves are stationary and reflect at the critical layer is boosted by $-M$ relative to the frame we defined in Equations (75).

We now consider the fate of a wavepacket that is trapped between the lower boundary and the critical layer. Figure 6 shows a set of wavefronts derived by integrating Equation (77) with red segments corresponding to propagation in the $+x$ direction and blue segments corresponding to propagation in the $-x$ direction. Consider a localized wavepacket at point A in Figure 6a. The wavevector of the wavepacket is oriented perpendicular to the wavefront, and as the wavepacket propagates towards point B, its wavevector is rotated by the shear. When the wavepacket reaches the critical layer at point C, it is reflected back towards point D, and the reflected wavepacket has a higher amplitude than the incident one (see Narayan et al. (1987) for the case of a rotating shear layer). After reflecting off the critical layer, the wavepacket propagates downward to point D, its wavevector continuing to be rotated in the same sense as before due to the shear. Finally the wavevector reaches the perfectly reflecting boundary at point E, whereupon the x -component of its wavevector is reflected and the cycle begins anew. It is thus clear that the repeating cycle A-E will lead to exponential amplification of the wavepacket, due to over-reflection at the critical layer.

The distance in y between points A and E is the wavelength of the longest wavelength mode, $\lambda_{\max,y}$, that can be trapped between the lower boundary and the critical layer. A trapped mode can have a wavelength shorter than $\lambda_{\max,y}$, as long as its wavelength satisfies the relation $\lambda_y = \lambda_{\max,y}/n$ where n is an integer. Thus, the relation for the wavenumber of the n -th trapped mode in the general case is

$$k_{n,y} = \frac{2\pi n}{\lambda_{\max,y}}. \quad (80)$$

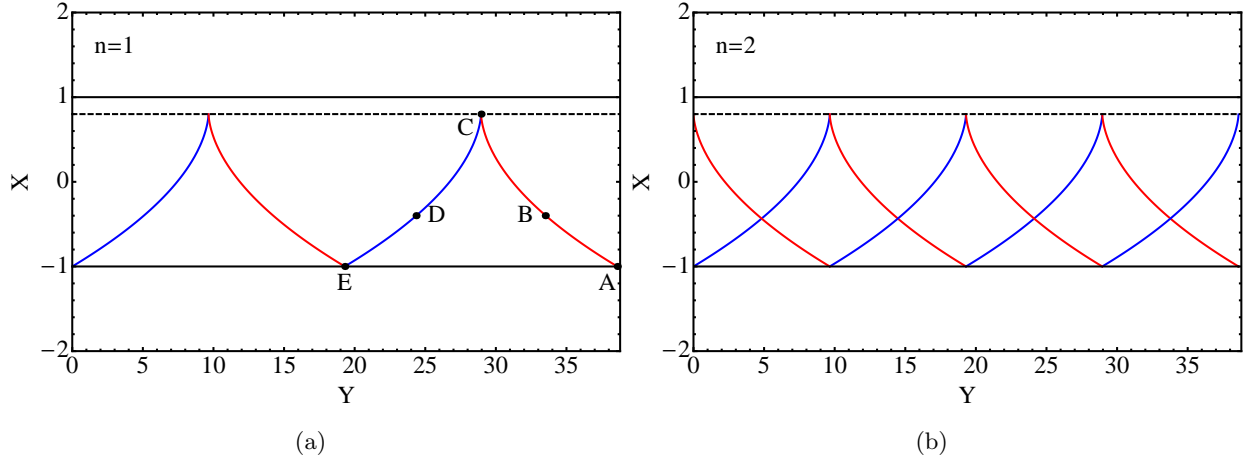


Fig. 6.— The $n = 1$ and $n = 2$ trapped modes for $M = 5$ and $\delta_{BL} = 1$. The lower black line denotes the solid lower boundary, the upper black line denotes the top of the shear layer, and the dashed black line denotes the critical layer. The red segments correspond to propagation in the $+x$ direction and the blue segments correspond to propagation in the $-x$ direction.

We indicate using arrows the values of $k_{n,y}$ for the first six trapped modes in panel (o) of Figure 3, and it is clear that they agree well with the locations of the peaks in the dispersion relation, which lends support for the over-reflection argument. We also plot the $n = 2$ case in Figure 6b and point out the similarity between the analytical curves in Figure 6 and the shape of the wavefronts from simulation D in Figure 5c.

We have discussed the radiation mechanism for $\epsilon = 1$ and the over-reflection mechanism for $\epsilon = 0$. We now discuss what happens in the more general case of $0 < \epsilon < 1$. As we can see from Figure 3, *both* mechanisms operate simultaneously for $0 < \epsilon < 1$. In this case, there is partial reflection at the lower boundary, and as ϵ goes from one to zero, less and less of the radiation can escape from the boundary layer region, so the radiation mechanism becomes weaker and weaker. This is evidenced by the decreasing size of the bump in the second and third columns of Figure 3 as ϵ goes to zero. For $\epsilon = 0$, the bump disappears entirely, and the radiation mechanism no longer operates. On the other hand, as ϵ goes from one to zero the reflection mechanism becomes stronger and stronger, since more and more of the energy is reflected at the lower boundary with total reflection at $\epsilon = 0$. Interestingly, there are still some small-scale wiggles in the dispersion relation, even for $\epsilon = 1$. This is because even if the density is everywhere uniform, radiation can still partially reflect off the discontinuity in the velocity derivative at $x = -1$ (Glatzel 1988). However, reflections off a discontinuity in the velocity derivative are quite weak, so the wiggles are small, and the radiation mechanism is dominant.

6. Discussion and Conclusions

We have studied supersonic shear instabilities that could drive the turbulence in the BLs of stars for which the disk is undisturbed by a magnetic field. Our study is aimed mainly at identifying the instabilities that lead to the formation of the BL when the disk just touches the surface of the star. The main result of our work is the identification of two types of instabilities that could operate in the BLs of such systems and had not been previously discussed in this context.

The first is an instability of a vortex sheet at high Mach number caused by gravity. Although the vortex sheet is stable above a critical Mach number, the addition of a small amount of gravity destabilizes it. We have found that the eigenfrequencies of the dispersion relation in the limit $G \rightarrow 0$ acquire a purely imaginary term, which is proportional to the small parameter G . This has the effect of making the upper branch unstable. We now consider whether the instability of the upper branch in the limit $G \rightarrow 0$ is likely to be relevant during the initiation of the BL, when one may expect the vortex sheet approximation to be valid. Redimensionalizing Equation (74), we obtain

$$\omega_1 \sim \Omega_K \epsilon^{1/2} i, \quad (81)$$

where Ω_K is the Keplerian velocity at the surface of the star. During the initiation of the BL, we expect disk material to be less dense than stellar material, which means that $\epsilon \lesssim 1$. It then follows from Equation (81) that the characteristic growth rate of the instability is $\lesssim \Omega_K$ and is independent of the wavenumber.

If the BL is radially thin, as would be expected during the initiation phase, then the growth rate given by Equation (81) is small compared to the shear rate $S \sim \Omega_K R_*/\delta_{BL} \gg \Omega_K$. Considering that S is the characteristic growth rate for shear instabilities, if there are other mechanisms for instability with growth rates proportional to S , they will quickly become dominant.

In particular, we have demonstrated that the growth rate of the sonic instability of a finite width shear layer at high Mach number is proportional to S . The sonic instability is similar in nature to the Papaloizou-Pringle instability in that both are global instabilities and cannot be derived from a local analysis. There are two destabilizing mechanisms for the sonic instability. The first corresponds to emission of radiation and gives instability over a broad range of wavenumbers. The second corresponds to over-reflection of trapped modes and results in sharply peaked, disconnected regions of instability in k -space. Because sonic instabilities operate on a much faster timescale than the gravity mechanism for a vortex sheet, this makes them an appealing candidate for the initial stages of boundary layer formation, when one might expect large shears to be present.

We mention that Alexakis et al. (2004) have considered the Miles instability (Miles 1957a) in the context of boundary layer formation. Specifically, they invoked the Miles instability to generate mixing of WD and stellar material and explain the enrichment in heavy elements observed in nova explosions. The Miles instability was proposed as a mechanism for generating waves over water at low wind speeds and operates through a resonant interaction between the wind and the water wave. Due to this interaction, a component of the pressure perturbation is created that is in phase

with the velocity of the air-water interface, and much like pumping a swing, swings up the interface to large amplitudes. However, the Miles instability was initially introduced as a way of explaining the formation of waves on water at weak wind speeds, for which the air-water interface is stable to the KH instability. During boundary layer formation, however, large shears are generated, so we are not in the weak wind regime, and the Miles instability is likely to be swamped by sonic instabilities.

There are two main astrophysical implications of our findings. First, we demonstrate that the initiation of the BL is likely to take only very short amount time after the first material from the disk arrives to the stellar surface. This is because the sonic instabilities that we explored in this paper have an extremely short growth rate, which is very weakly dependent on the density contrast between the disk and stellar material.¹ Thus, mixing of the two fluids starts almost immediately after they come into contact.

Second, given the efficiency with which the sonic instability operates, it is likely that it may play important role also in more developed phases of the BL evolution. As long as the BL possesses some effective "boundaries" (e.g. sharp changes in the velocity of density behavior) and the gas flow within it is supersonic the purely hydrodynamic sonic instabilities are going to operate in it potentially providing means for continuing mixing and angular momentum transport inside the layer. Future numerical calculations capable of following the nonlinear development of sonic instabilities should be able to address this issue.

We are grateful to Jim Stone for useful discussions. The financial support for this work is provided by the Sloan Foundation and NASA grant NNX08AH87G.

REFERENCES

- Abramowitz, M., & Stegun, I. A. 1972, Handbook of Mathematical Functions, New York: Dover, 1972,
- Alexakis, A., Young, Y., & Rosner, R. 2002, Phys. Rev. E, 65, 026313
- Alexakis, A., Calder, A. C., Dursi, L. J., et al. 2004, Physics of Fluids, 16, 3256
- Armitage, P. J. 2002, MNRAS, 330, 895
- Balbus, S. A., & Hawley, J. F. 1991, ApJ, 376, 214
- Balsara, D. S., Fisker, J. L., Godon, P., & Sion, E. M. 2009, ApJ, 702, 1536
- Bergeron, P., Saffer, R. A., & Liebert, J. 1992, ApJ, 394, 228

¹This statement is not true for the supersonic KH instability with gravity investigated in §4, see Equation (74).

- Blumen, W., Drazin, P. G., & Billings, D. F. 1975, *Journal of Fluid Mechanics*, 71, 305
- Chang, I.-D., & Russell, P. E. 1965, *Physics of Fluids*, 8, 1018
- Chimonas, G. 1970, *Journal of Fluid Mechanics*, 43, 833
- Choudhury, S. R., & Lovelace, R. V. E. 1984, *ApJ*, 283, 331
- Cowling, T. G. 1941, *MNRAS*, 101, 367
- Crawford, J. A., & Kraft, R. P. 1956, *ApJ*, 123, 44
- Fejer, J. A., & Miles, J. W. 1963, *Journal of Fluid Mechanics*, 15, 335
- Fisker, J. L., & Balsara, D. S. 2005, *ApJ*, 635, L69
- Fujimoto, M. Y. 1987, *A&A*, 176, 53
- Fujimoto, M. Y. 1988, *A&A*, 198, 163
- Gerwin, R. A. 1968, *Reviews of Modern Physics*, 40, 652
- Ghosh, P., & Lamb, F. K. 1978, *ApJ*, 223, L83
- Gilfanov, M., Revnivtsev, M., & Molkov, S. 2003, *A&A*, 410, 217
- Glatzel, W. 1988, *MNRAS*, 231, 795
- Godon, P. 1995, *MNRAS*, 277, 157
- Hachisu, I. 1986, *ApJS*, 62, 461
- Hanawa, T. 1987, *A&A*, 179, 383
- Hatanaka, H. 1949, *J. Soc. Sci. Culture*, 2, 3
- Howard, L. N. 1961, *Journal of Fluid Mechanics*, 10, 509
- Inogamov, N. A., & Sunyaev, R. A. 1999, *Astronomy Letters*, 25, 269
- Kenyon, S. J., Hartmann, L., & Hewett, R. 1988, *ApJ*, 325, 231
- Kippenhahn, R., & Thomas, H.-C. 1978, *A&A*, 63, 265
- Kley, W., & Hensler, G. 1987, *A&A*, 172, 124
- Kley, W. 1989, *A&A*, 208, 98
- Kley, W. 1989, *A&A*, 222, 141
- Kluźniak, W. 1987, Ph.D. Thesis,

- Koldoba, A. V., Romanova, M. M., Ustyugova, G. V., & Lovelace, R. V. E. 2002, *ApJ*, 576, L53
- Landau, L. 1944, *C.R. Acad. Sci. U.S.S.R.*, 44, 139
- Livio, M., & Pringle, J. E. 1992, *MNRAS*, 259, 23P
- Lynden-Bell, D., & Pringle, J. E. 1974, *MNRAS*, 168, 603
- Miles, J. W. 1957, *Journal of Fluid Mechanics*, 3, 185
- Miles, J. W. 1957, *Acoustical Society of America Journal*, 29, 226
- Miles, J. W. 1958, *Journal of Fluid Mechanics*, 4, 538
- Miles, J. W. 1961, *Journal of Fluid Mechanics*, 10, 496
- Miles, J. W. 1965, *Physics of Fluids*, 8, 1754
- Narayan, R. 1992, *ApJ*, 394, 261
- Narayan, R., Goldreich, P., & Goodman, J. 1987, *MNRAS*, 228, 1
- Pai, S. I. 1954, *J. Aero. Sci.* 21, 325
- Papaloizou, J. C. B., & Pringle, J. E. 1984, *MNRAS*, 208, 721
- Patterson, J. 1984, *ApJS*, 54, 443
- Piro, A. L., & Bildsten, L. 2004, *ApJ*, 610, 977
- Piro, A. L., & Bildsten, L. 2007, *ApJ*, 663, 1252
- Popham, R., & Narayan, R. 1992, *ApJ*, 394, 255
- Popham, R., Narayan, R., Hartmann, L., & Kenyon, S. 1993, *ApJ*, 415, L127
- Popham, R., & Narayan, R. 1995, *ApJ*, 442, 337
- Pringle, J. E. 1977, *MNRAS*, 178, 195
- Pringle, J. E. 1981, *ARA&A*, 19, 137
- Pringle, J. E., & King, A. R. 2007, *Astrophysical flows* by J. E. Pringle, A.R. King; Cambridge University Press, 2007.
- Ray, T. P. 1982, *MNRAS*, 198, 617
- Shakura, N. I., & Sunyaev, R. A. 1973, *A&A*, 24, 337
- Shakura, N. I., & Sunyaev, R. A. 1988, *Advances in Space Research*, 8, 13

- Shtemler, Y. M., Mond, M., Cherniavskii, V., Golbraikh, E., & Nissim, Y. 2008, *Physics of Fluids*, 20, 094106
- Spruit, H. C. 1999, *A&A*, 349, 18
- Stone, J. M., Gardiner, T. A., Teuben, P., Hawley, J. F., & Simon, J. B. 2008, *ApJS*, 178, 137
- Sung, C.-H. 1974, *A&A*, 33, 99
- Tassoul, J.-L. 2000, *Stellar rotation / Jean-Louis Tassoul*. Cambridge ; New York : Cambridge University Press, 2000. (Cambridge astrophysics series ; 36),
- Vallis, G. K. 2006, *Atmospheric and Oceanic Fluid Dynamics*, by Geoffrey K. Vallis, pp. 770. Cambridge University Press, November 2006. ISBN-10: 0521849691. ISBN-13: 9780521849692,
- Wheatley, P. J., Mauche, C. W., & Mattei, J. A. 2003, *MNRAS*, 345, 49

A. Reduction of Equations

Defining $S \equiv \varpi d\Omega/d\varpi$ to be the shear rate, and assuming $\delta_{BL} \ll R_*$ and $\Omega_* \ll \Omega_K$ we have that $2B \approx S \sim \Omega_K R_*/\delta_{BL} \gg \Omega_K$. We next note that $|\bar{\omega}|^2 \geq (\Im[\bar{\omega}])^2$ with exact equality at the location of a critical layer, where $\Re[\bar{\omega}] = 0$. According to Chimonas (1970), the growth rate of the fastest growing mode in a plane parallel stratified shear flow is of the order

$$\Im[\omega] \sim \frac{1}{4}S^2 - N^2, \quad (\text{A1})$$

where N is the Brunt-Väisälä frequency (Equation (56)). If we assume that shear instabilities provide the turbulence in the BL, then we can estimate that $|\bar{\omega}|^2 \gtrsim S^2$. Using this estimate on the left hand side of Equation (15), we find that the first term, $\bar{\omega}^2$, dominates the third term, $\kappa^2 \approx 2\Omega S$ by a factor of $R_*/\delta_{BL} \gg 1$, so we can ignore the third term. Next, we compare the second to last term $\bar{\omega}\bar{g}/s^2$ to the last term $2\Omega m/\varpi$ on the right hand side of Equation (15). Defining $h_s \equiv s^2/\bar{g}$, dividing the second to last term by the last term, and ignoring constants of order unity we have $\bar{\omega}R_*/h_s m\Omega \gtrsim SR_*/h_s m\Omega \sim R_*^2/h_s \delta_{BL} m$. Next, we make the additional reasonable assumption that the fastest growing mode has $m/R_* \sim h_s^{-1}$, since h_s is of order the scale height and sets the natural length scale in the problem. Continuing our line of reasoning, we then have $R_*^2/h_s \delta_{BL} m \sim R_*/\delta_{BL} \gg 1$. This means that the last term in equation (15) is negligible compared to the second to last term and can be ignored. Finally, we compare the first term, $C_L \bar{\omega}$, and the second term, $2Bm/\varpi$, on the right hand side of Equation (14). Dividing the first term by the second term, using $2B \approx S$, $|\bar{\omega}|^2 \gtrsim S^2$ and $m/R_* \sim h_s^{-1}$, and noting that $C_L \sim h_s^{-1}$, we have

$C_L \bar{\omega} R_*/mS \gtrsim h_s S/h_s S \sim 1$. Thus, both terms can potentially be of comparable magnitude and both must be retained.

Keeping only the dominant terms for $\delta_{BL} \ll R_*$, using $\varpi \approx R_*$, and assuming that $\rho'/\rho \gg R_*^{-1}$ and $\delta u'/\delta u \gg R_*^{-1}$, Equations (14) and (15) finally reduce to Equations (16) and (17).

B. Generalized Rayleigh Equation and Boundary Conditions

B.1. Derivation of the Generalized Rayleigh Equation

We start with Equations (19) and (20). Using the definitions from §2, Equation (19) can be written as

$$\delta u' + C_1(x)\delta u = C_2(x) \quad (\text{B1})$$

$$C_1(x) = -(k_g + W'/W) \quad (\text{B2})$$

$$C_2(x) = i(1 - W^2/s^2)k_y \delta P/\rho W, \quad (\text{B3})$$

and similarly Equation (20) can be written as

$$\delta P' + C_3(x)\delta P = C_4(x) \quad (\text{B4})$$

$$C_3(x) = k_g \quad (\text{B5})$$

$$C_4(x) = -i\rho(k_y^2 W^2 + g(k_g + k_s))\delta u/k_y W. \quad (\text{B6})$$

We can use the integrating factor method of solving first order differential equations to make a change of variables and get rid of the δu term in Equation (B1) and the δP term in Equation (B4). Making these changes of variable, we have

$$\delta q' = \frac{(1 - W^2/s^2)k_y \delta P}{\rho W^2 f}, \quad \delta q \equiv (iWf)^{-1} \delta u \quad (\text{B7})$$

$$\delta \tilde{P}' = -\frac{if\rho(k_y^2 W^2 + g(k_g + k_s))\delta u}{k_y W}, \quad \delta \tilde{P} \equiv f\delta P. \quad (\text{B8})$$

We can combine Equations (B7) and (B8) into a single equation for δq :

$$\left(\frac{\tilde{\rho} W^2 \delta q'}{1 - W^2/s^2} \right)' = \tilde{\rho}(k_y^2 W^2 + g(k_g + k_s))\delta q. \quad (\text{B9})$$

This is the same basic form as Chimonas (1970). Since Equation (B9) is a second order differential equation for δq , we can convert it to standard form (get rid of the first order term) with the change of variable

$$\delta \phi = \tilde{W} \delta q/k_y. \quad (\text{B10})$$

Making this change of variable yields Equation (21) which is the generalized Rayleigh equation (Alexakis et al. 2002).

B.2. Derivation of the Boundary Conditions at the Interface

We present here a physically motivated derivation of the interfacial boundary conditions, Equations (31) and (32). The two classical boundary conditions for the vortex sheet that should be satisfied at the interface are (1) that the two fluids should stay in contact at the interface, and (2) that the force exerted on the lower fluid by the upper fluid is equal and opposite to the force exerted on the upper fluid by the lower fluid. These can be expressed as

$$\delta\xi_+ = \delta\xi_- \quad (\text{B11})$$

$$\Delta P_+ = \Delta P_-, \quad (\text{B12})$$

where $\delta\xi$ is the displacement of the interface in the x -direction, and Δ denotes the Lagrangian differential. However, we must formulate both of these boundary conditions in terms of the generalized streamfunction perturbation $\delta\phi$.

We begin with the condition $\delta\xi_+ = \delta\xi_-$. We start with the relation

$$\frac{D\delta\xi}{Dt} = -i(\omega - k_y V_y)\delta\xi = \delta u, \quad (\text{B13})$$

where D/Dt , denotes the Lagrangian derivative. From Equations (B11) and (B13) we have

$$\frac{\delta u_+}{\omega - k_y V_y} = \frac{\delta u_-}{\omega + k_y V_y}. \quad (\text{B14})$$

Using the definitions of $\delta\phi$, \tilde{W} , and $\tilde{\rho}$ given in §2, and noting that $\tilde{\rho} = \rho$ at the interface ($x = 0$), we immediately get Equation (31):

$$\frac{\delta\phi_+}{\tilde{W}_+} = \frac{\delta\phi_-}{\tilde{W}_-}. \quad (\text{B15})$$

For the second boundary condition, we begin by writing

$$\Delta P = \delta P - g\rho\delta\xi. \quad (\text{B16})$$

Using Equation (B7) we can substitute for δP in terms of δq , which gives at the interface

$$\frac{\tilde{W}_+^2}{k_y}\delta q'_+ - g_+\rho_+\delta\xi_+ = \frac{\tilde{W}_-^2}{k_y}\delta q'_- - g_-\rho_-\delta\xi_-. \quad (\text{B17})$$

Using Equations (B13), (B7), and (B10) to substitute for $\delta\xi$, δq , and δu in terms of $\delta\phi$, we arrive at Equation (32):

$$\tilde{W}_+\delta\phi'_+ - \tilde{W}'_+\delta\phi_+ - \frac{g_+\tilde{\rho}_+\delta\phi_+}{\tilde{W}_+} = \tilde{W}_-\delta\phi'_- - \tilde{W}'_-\delta\phi_- - \frac{g_-\tilde{\rho}_-\delta\phi_-}{\tilde{W}_-}. \quad (\text{B18})$$

C. Finite Width Shear Layer

We derive here the dispersion relation for a finite width shear layer in the absence of gravity and for a constant shear. Our analysis extends the work of Glatzel (1988) to arbitrary density ratios above and below the shear layer. We will use his notation in this section and consider the pressure perturbation δP rather than the generalized stream function $\delta\phi$. Where appropriate, we describe how to transform the results back into the notation used in the body of the text.

C.1. Setup of the Problem

Consider the velocity profile

$$V(x) = \begin{cases} -1, & x < -1 \\ x, & -1 \leq x \leq 1 \\ 1, & x > 1, \end{cases} \quad (\text{C1})$$

and the density profile

$$\rho(x) = \begin{cases} \rho_-, & x < -1 \\ \rho_0, & -1 \leq x \leq 1 \\ \rho_+, & x > 1. \end{cases} \quad (\text{C2})$$

The adiabatic index and equilibrium pressure are everywhere constant so we have $\rho_- s_-^2 = \rho_+ s_+^2 = \rho_0 s_0^2$. The perturbations are assumed to be of the form $\delta P = \delta f(x) \exp[i(k_y y - \omega t)]$. We define $M = 1/s_0$ to be the Mach number at $x = 1$ inside the shear layer. We also define

$$\epsilon_- = \rho_0/\rho_- \quad (\text{C3})$$

$$\epsilon_+ = \rho_0/\rho_+ \quad (\text{C4})$$

and adopt the following quantities from Glatzel (1988)

$$\bar{\sigma} \equiv W = -\frac{\bar{\omega}}{k_y} \quad (\text{C5})$$

$$Q \equiv \bar{\sigma}^{-1/2} \delta P \quad (\text{C6})$$

$$\zeta = ik_y M \bar{\sigma}^2 \quad (\text{C7})$$

$$\chi = \frac{i k_y}{4 M} \quad (\text{C8})$$

$$\mu = \frac{3}{4}. \quad (\text{C9})$$

Glatzel (1988) has shown that Q satisfies Whittaker's equation

$$\frac{d^2 Q}{d\zeta^2} + \left(-\frac{1}{4} + \frac{\chi}{\zeta} + \frac{1/4 - \mu^2}{\zeta^2} \right) Q = 0 \quad (\text{C10})$$

and inside the shear layer has the solution

$$Q = c_1 M_{\chi, \mu}(\zeta) + c_2 M_{\chi, -\mu}(\zeta), \quad (\text{C11})$$

where c_1 and c_2 are constants and $M_{\chi, \mu}(\zeta)$ is a Whittaker function. Outside the shear layer the velocity is constant, and the perturbation can be written as

$$Q \propto \begin{cases} \exp [\pm k_y (1 - \epsilon_-^{-1} M^2 \bar{\sigma}^2)^{1/2} x], & x < -1 \\ \exp [\pm k_y (1 - \epsilon_+^{-1} M^2 \bar{\sigma}^2)^{1/2} x], & x > 1 \end{cases} \quad (\text{C12})$$

The signs in the exponentials should be chosen based on the condition of outgoing waves (§3.1).

C.2. Dispersion Relation

To derive the dispersion relation, we must apply the contact and pressure continuity boundary conditions at $x = \pm 1$ (Appendix B.2). Since the velocity and hence $\bar{\sigma}$ are everywhere continuous, the pressure continuity boundary conditions at $x = \pm 1$ are simply

$$Q_{\text{in}} = Q_{\text{out}} \quad (\text{C13})$$

where the subscripts “in” and “out” denote evaluation of a quantity inside or outside the shear layer, respectively. Using the expression (Glatzel 1988)

$$\delta u = \frac{i}{k \rho \bar{\sigma}} \delta P', \quad (\text{C14})$$

the contact boundary conditions at $x = \pm 1$ can be written as

$$\delta u_{\text{in}} = \delta u_{\text{out}} \quad (\text{C15})$$

$$\rho_{\text{out}} \delta P'_{\text{in}} = \rho_{\text{in}} \delta P'_{\text{out}} \quad (\text{C16})$$

$$\frac{1}{4\zeta} + \frac{1}{Q_{\text{in}}} \frac{dQ_{\text{in}}}{d\zeta} = \pm \frac{\rho_{\text{in}}/\rho_{\text{out}}}{2} \left(\frac{\rho_{\text{out}}}{\rho_{\text{in}}} - 4 \frac{\chi}{\zeta} \right)^{1/2}. \quad (\text{C17})$$

In deriving the expression (C17), we have made use of relations (C5-C8), and also the results (C12) and (C13). The sign in Equation (C17) should be chosen on the basis of outgoing waves, and the lower sign should be chosen at $x = 1$ and the upper sign at $x = -1$. We also point out that $\rho_{\text{in}}/\rho_{\text{out}} = \epsilon_{\pm}$ at $x = \pm 1$.

Next, we substitute Equation (C11) into Equation (C17) at $x = \pm 1$, and set $c_1 = 1$, which sets the normalization. Using the property of the Whittaker function (Abramowitz & Stegun 1972) that

$$\zeta \frac{dM_{\chi, \mu}}{d\zeta} = \left(\frac{\zeta}{2} - \chi \right) M_{\chi, \mu} + \left(\frac{1}{2} + \chi + \mu \right) M_{\chi+1, \mu}, \quad (\text{C18})$$

we can derive the dispersion relation

$$\frac{\left[1 - 4\chi + 2\zeta_+ + 2\epsilon_+\zeta_+ \left(\epsilon_+^{-1} - 4\frac{\chi}{\zeta_+}\right)^{1/2}\right] M_{\chi, \frac{3}{4}}(\zeta_+) + (4\chi + 5)M_{\chi+1, \frac{3}{4}}(\zeta_+)}{\left[1 - 4\chi + 2\zeta_+ + 2\epsilon_+\zeta_+ \left(\epsilon_+^{-1} - 4\frac{\chi}{\zeta_+}\right)^{1/2}\right] M_{\chi, -\frac{3}{4}}(\zeta_+) + (4\chi - 1)M_{\chi+1, -\frac{3}{4}}(\zeta_+)} = \frac{\left[1 - 4\chi + 2\zeta_- - 2\epsilon_-\zeta_- \left(\epsilon_-^{-1} - 4\frac{\chi}{\zeta_-}\right)^{1/2}\right] M_{\chi, \frac{3}{4}}(\zeta_-) + (4\chi + 5)M_{\chi+1, \frac{3}{4}}(\zeta_-)}{\left[1 - 4\chi + 2\zeta_- - 2\epsilon_-\zeta_- \left(\epsilon_-^{-1} - 4\frac{\chi}{\zeta_-}\right)^{1/2}\right] M_{\chi, -\frac{3}{4}}(\zeta_-) + (4\chi - 1)M_{\chi+1, -\frac{3}{4}}(\zeta_-)}. \quad (\text{C19})$$

Using the relation between the confluent hypergeometric function and the Whittaker function (Glatzel 1988), Equation (C19) can be written in terms of the confluent hypergeometric function as

$$\bar{\sigma}_+^3 \frac{\left[1 - 4\chi + 2\zeta_+ + 2\epsilon_+\zeta_+ \left(\epsilon_+^{-1} - 4\frac{\chi}{\zeta_+}\right)^{1/2}\right] {}_1F_1\left(\frac{5}{4} - \chi, \frac{5}{2}, \zeta_+\right) + (4\chi + 5){}_1F_1\left(\frac{1}{4} - \chi, \frac{5}{2}, \zeta_+\right)}{\left[1 - 4\chi + 2\zeta_+ + 2\epsilon_+\zeta_+ \left(\epsilon_+^{-1} - 4\frac{\chi}{\zeta_+}\right)^{1/2}\right] {}_1F_1\left(-\frac{1}{4} - \chi, -\frac{1}{2}, \zeta_+\right) + (4\chi - 1){}_1F_1\left(-\frac{5}{4} - \chi, -\frac{1}{2}, \zeta_+\right)} = \bar{\sigma}_-^3 \frac{\left[1 - 4\chi + 2\zeta_- - 2\epsilon_-\zeta_- \left(\epsilon_-^{-1} - 4\frac{\chi}{\zeta_-}\right)^{1/2}\right] {}_1F_1\left(\frac{5}{4} - \chi, \frac{5}{2}, \zeta_-\right) + (4\chi + 5){}_1F_1\left(\frac{1}{4} - \chi, \frac{5}{2}, \zeta_-\right)}{\left[1 - 4\chi + 2\zeta_- - 2\epsilon_-\zeta_- \left(\epsilon_-^{-1} - 4\frac{\chi}{\zeta_-}\right)^{1/2}\right] {}_1F_1\left(-\frac{1}{4} - \chi, -\frac{1}{2}, \zeta_-\right) + (4\chi - 1){}_1F_1\left(-\frac{5}{4} - \chi, -\frac{1}{2}, \zeta_-\right)}. \quad (\text{C20})$$

Equation (C20) is a generalization of the dispersion relations considered by Glatzel (1988). For instance, taking $\epsilon_{\pm} \rightarrow 0$ we recover his dispersion relation (5.23) for the reflecting boundary condition $\delta u(x = \pm 1) = 0$, taking $\epsilon_{\pm} \rightarrow \infty$ we recover his dispersion relation (5.24) for a vacuum boundary condition $\delta P(x = \pm 1) = 0$, and taking $\epsilon_{\pm} = 1$ we recover his dispersion relation (5.38) for an infinite fluid with uniform density everywhere.

C.3. The Vortex Sheet Limit

We can show that Equation (C20) reduces to the dispersion relation for the vortex sheet, (Equation (40)), by taking the limit $k_y \rightarrow 0$. In this limit, $\zeta \rightarrow 0$ and $\chi \rightarrow 0$, but $\bar{\sigma}$, the phase speed in the comoving frame, is finite, and

$$4\frac{\chi}{\zeta} = (M^2\bar{\sigma}^2)^{-1} \quad (\text{C21})$$

is also finite. We also note the property of the hypergeometric function that in the limit $\zeta \rightarrow 0$

$${}_1F_1(l, m, \zeta) = 1 + \frac{l}{m}\zeta + \mathcal{O}(\zeta^2). \quad (\text{C22})$$

Using these relations, Equation (C20) can be reduced to the form

$$\bar{\sigma}_+^2 \epsilon_- (M^2 \bar{\sigma}_-^2 \epsilon_-^{-1} - 1)^{1/2} = \bar{\sigma}_-^2 \epsilon_+ (M^2 \bar{\sigma}_+^2 \epsilon_+^{-1} - 1)^{1/2} \quad (\text{C23})$$

Equation (40) can then be obtained by setting $\epsilon_+ = 1$, $\epsilon_- = \epsilon$, and using the relation $M = 1/s_+$.